Modeling the Miocene climatic optimum: Ocean circulation

N. Herold,[1] M. Huber,[2] R. D. Müller,[1] and M. Seton[1]

Received 10 August 2010; revised 22 November 2011; accepted 22 December 2011; published 21 February 2012.

[1] Ocean circulation is investigated using the Community Climate System Model 3 (CCSM3) forced with early to middle Miocene (~20–14 Ma) topography, bathymetry, vegetation and modern CO_2. Significant bottom water formation is modeled in the Weddell Sea along with intermediate North Component Water formation in the North Atlantic. This is attributed primarily to stronger- and weaker-than-modern convective preconditioning in the Weddell and Labrador Seas, respectively. Global meridional overturning and gyre circulation is weaker in the Miocene due to weaker midlatitude westerlies in the southern hemisphere, caused by lowering of the meridional surface temperature gradient, in addition to regional influences on convection. Subsurface temperatures in the Miocene are significantly higher in the far North Atlantic, Greenland-Norwegian Seas and Arctic basin compared to the present. Ocean heat transport is symmetrical about the equator and resembles that simulated for late Cretaceous and early Cenozoic climates, suggesting the northern hemisphere dominated ocean heat transport active today developed after the middle Miocene. Simulated deep water warming in the Miocene is more than an order of magnitude lower than indicated by proxies. This discrepancy is not reconciled by higher CO_2 due to the persistence of sea-ice at sites of deep water formation. This suggests that either the CCSM3 is insufficiently sensitive to Miocene boundary conditions, greater greenhouse forcing existed than is currently reconstructed, or that proxy records of warming are exaggerated. Given the diversity of global Miocene proxy records and their near-unanimous estimate of a significantly warmer Earth, the first two options are more likely.

Citation: Herold, N., M. Huber, R. D. Müller, and M. Seton (2012), Modeling the Miocene climatic optimum: Ocean circulation, *Paleoceanography*, *27*, PA1209, doi:10.1029/2010PA002041.

1. Introduction

[2] Global temperature during the Miocene climatic optimum was significantly higher than present [e.g., *Zachos et al.*, 2008], though the causes of this warmth are controversial. Interpretations of paleoceanographic records suggest that Miocene warmth was linked to changes in ocean circulation [*Flower and Kennett*, 1994; *Lagabrielle et al.*, 2009; *Poore et al.*, 2006; *Ramsay et al.*, 1998; *Schnitker*, 1980; *Shevenell and Kennett*, 2004; *Woodruff and Savin*, 1989] although cause and effect are impossible to establish without a suitable physical framework. Ocean-only and coupled ocean–atmosphere modeling has been applied in a number of studies to develop an understanding of these changes and place them within a broader Cenozoic context [*Barron and Peterson*, 1991; *Bice et al.*, 2000; *Brady et al.*, 1998; *Huber and Sloan*, 2001; *Najjar et al.*, 2002; *Nong et al.*, 2000; *Otto-Bliesner et al.*, 2002]. While coupled atmosphere–ocean modeling has demonstrated that ocean circulation changes did not dominate global temperature change throughout the Cenozoic [*Huber and Sloan*, 2001], sensitivity studies have shown that ocean gateway evolution had large regional [*Sijp and England*, 2004; *Sijp et al.*, 2009] and distal [*Cane and Molnar*, 2001] effects on surface climate and deep ocean temperatures. The uncertainty surrounding the role of CO_2 during the Miocene [cf. *Kürschner et al.*, 2008; *Pagani et al.*, 1999] as well as the dynamics of the Miocene oceans [cf. *Woodruff and Savin*, 1989; *Wright et al.*, 1992] makes investigating changes in ocean circulation during this period important.

[3] Previous simulations relevant to early to middle Miocene ocean circulation have either not included synchronous coupling of atmospheric processes [*Barron and Peterson*, 1991; *Bice et al.*, 2000; *Butzin et al.*, 2011; *Nisancioglu et al.*, 2003] or have not incorporated realistic vegetation, topography and bathymetry [*Nong et al.*, 2000; *Sijp and England*, 2004; *Toggweiler and Bjornsson*, 2000; *von der Heydt and Dijkstra*, 2006]. However, these studies clearly demonstrate significant changes in ocean circulation compared to the present. *Toggweiler and Bjornsson* [2000] show that opening of the Drake Passage leads to high latitude cooling in the southern hemisphere and warming in the northern hemisphere. This result was built upon by *Sijp and England* [2004] who examine North Atlantic Deep Water formation strength as a function of Drake Passage depth. *Von der Heydt and Dijkstra* [2006] find that widening of Southern Ocean gateways and closure of the

[1]EarthByte Group, School of Geosciences, University of Sydney, Sydney, New South Wales, Australia.
[2]Earth and Atmospheric Sciences, Purdue University, West Lafayette, Indiana, USA.

0883-8305/12/2010PA002041

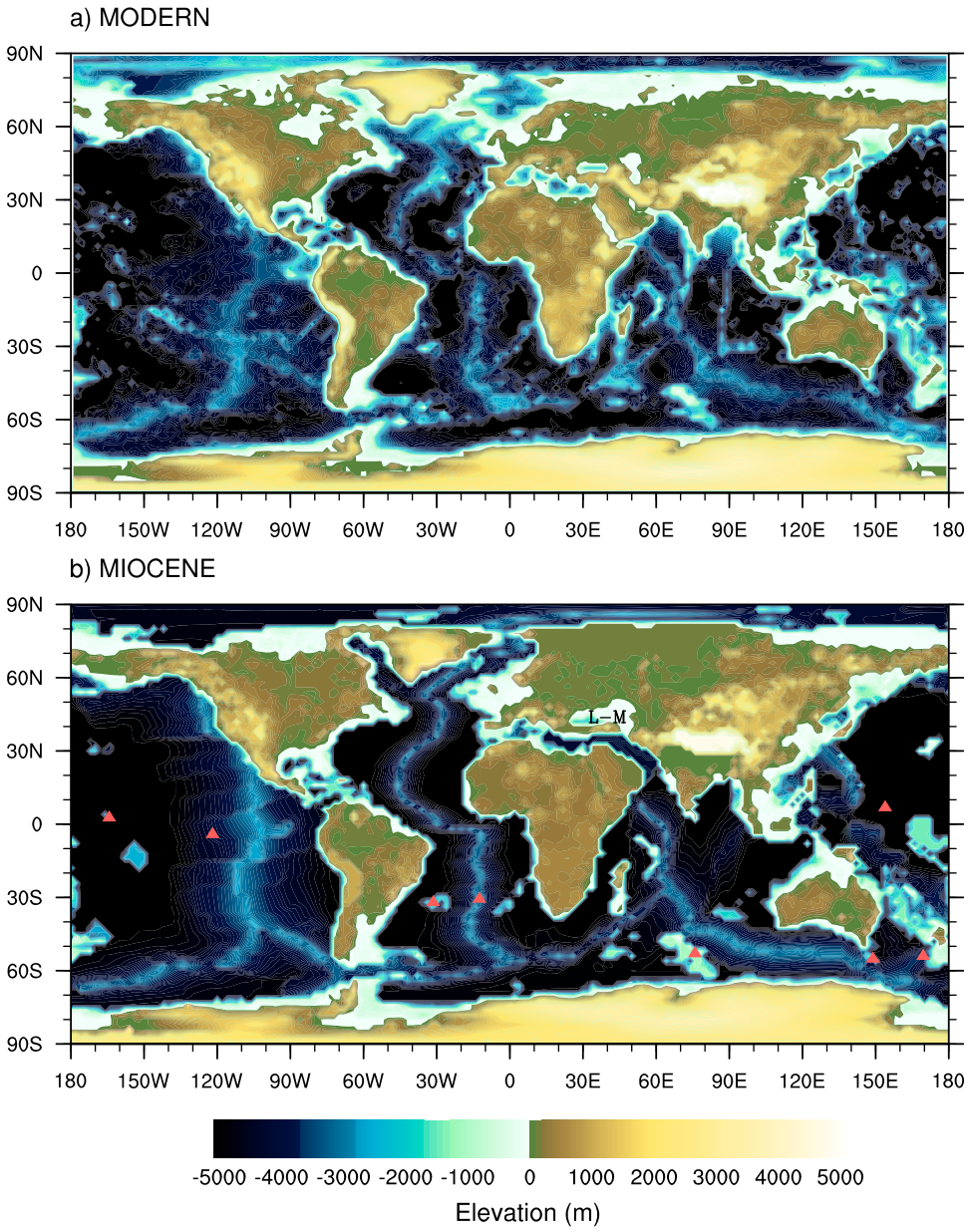

Figure 1. (a) Modern and (b) Miocene topography and bathymetry. Red triangles indicate the location of deep water temperature estimates (Table 2). L-M indicates Lago-Mare.

Tethys gateway during the Oligocene-Miocene transition lead to a reversal of Panama throughflow.

[4] *Micheels et al.* [2011] recently used a coupled atmosphere–ocean model with reconstructed boundary conditions to examine mechanisms of heat transport in the late Miocene, focusing on atmospheric characteristics. They find that a lower-than-present northern hemisphere ocean heat transport due to weaker North Atlantic Deep Water formation is compensated by an increase in atmospheric heat transport. Thus studies not utilizing an atmosphere–ocean modeling framework may overestimate the impact of altered ocean heat transport on past or future climates.

[5] In this study we use the Community Climate System Model 3 (CCSM3) to explore the effects of global Miocene boundary conditions on ocean circulation, in comparison with a control simulation forced with modern boundary conditions. Specifically, we investigate changes in mixed-layer characteristics and water mass formation. A significant improvement over the majority of previous studies is the implementation of reconstructed physical boundary conditions (vegetation, topography and bathymetry) in a coupled atmosphere–ocean modeling framework. In this sense, the purpose of this study is to present a first order approximation of early to middle Miocene ocean circulation simulated independently of assumptions of atmospheric heat transport and surface conditions, while at the same time evaluating the ability of a well-known coupled climate model in simulating a pre-Quaternary ocean state significantly warmer than the

present. A companion study examines results from the same simulations in the context of land and atmosphere climate [*Herold et al.*, 2011].

2. Model Description

[6] The CCSM3 consists of four component models of the atmosphere, ocean, land and sea-ice, each communicating via a coupler [*Collins et al.*, 2006]. Both the land and atmosphere models share a horizontal T31 spectral grid, representing a resolution of 3.75° × ~3.75° in longitude and latitude, respectively. The ocean model utilizes a z-coordinate system with 25 vertical levels and is configured with the Gent-McWilliams scheme for eddy parameterization. Vertical mixing is handled with the KPP scheme and all tunable parameters for the mixing schemes are held at the standard, modern values used in this low resolution version of the model [*Yeager et al.*, 2006]. The ocean and sea-ice models operate on a horizontal stretched grid of approximately 3° × ~1.5° in longitude and latitude, respectively, with coarser resolution at middle latitudes and finer meridional resolution at the equator. Due to numerical limitations the North Pole is centered over Greenland in the ocean and sea-ice model grids. Conservation of salinity between the atmosphere and ocean is achieved via a river transport scheme which moves excess water from land to ocean grid points according to topographic relief. The CCSM3 has been previously utilized for past [*Ali and Huber*, 2010; *Kiehl and Shields*, 2005; *Liu et al.*, 2009; *Shellito et al.*, 2009], present and future climate simulations [*Meehl et al.*, 2007].

3. Experiment Design

[7] For our Miocene simulation topography and bathymetry are adapted from *Herold et al.* [2008] (Figure 1) and vegetation is prescribed based on *Wolfe* [1985] with improvements based on more recent scholarship. The most important amendment is that ice is prescribed to the majority of East Antarctica. This is consistent with evidence suggesting a large ice sheet existed on the continent [*Pekar and DeConto*, 2006] with tundra likely occupying coastal regions [*Warny et al.*, 2009]. N_2O and CH_4 are set to pre-industrial concentrations of 270 ppb and 760 ppb, respectively. The solar constant is set to 1365 W/m^2 (compared to 1367 W/m^2 for modern CCSM3 simulations) and obliquity, eccentricity and precession are set to values appropriate for 1950. As CO_2 during the Miocene is controversial [cf. *Kürschner et al.*, 2008; *Pagani et al.*, 1999] we prescribe a concentration of 355 ppmv, midway between the majority of estimates and the same as modern day CCSM3 simulations. This choice simplifies comparison with the modern control case. Initial ocean temperatures and salinities are based on modern global depth averages. Based on the depth-integrated ocean mean temperature the simulation equilibrates after approximately 800 years. The model is run for a further 300 years, at which point global mean ocean temperature varies by <0.01°C per century. The final 100 years is used for analysis. We compare our Miocene case to a control case forced with modern boundary conditions and greenhouse gas concentrations appropriate for 1990, including a CO_2 of 355 ppmv.

4. Results

4.1. Mixed-Layer Temperatures, Salinities and Currents

[8] The distribution of mixed-layer temperatures and velocities are largely similar in the Miocene and modern simulations, with a few notable exceptions. Poleward of 45°N in the North Atlantic, temperatures in the central and eastern basin are up to 4°C cooler in the Miocene due to weakness of the North Atlantic Drift at these latitudes (Figure 2c). This cooling is consistent with the effects of an open Panama gateway and the magnitude of temperature change lies between previous sensitivity experiments [cf. *Klocker et al.*, 2005; *Lunt et al.*, 2008]. Conversely, temperatures along the east coast of Greenland are 1–2°C higher in the Miocene (cf. Figures 2a and 2b). In the Miocene equatorial Pacific a more pronounced zonal temperature distribution is simulated, with an intensified cold tongue stretching into the Western Pacific Warm Pool, straddled to the north and south by eastward stretching warm tongues (Figure 2). Intensification of the cold tongue is associated with stronger upwelling into the base of the mixed-layer (not shown). A zonal band of warming in the Miocene far Northwest Pacific (Figure 2c) occurs in conjunction with more intense vertical mixing (discussed below), though this mixing is limited to depths of less than 1 km. In general, the extra-tropical latitudes of the North Pacific, South Atlantic and Indian Oceans warm considerably compared to the present, at the expense of the tropics and far North Atlantic (Figure 2c).

[9] Salinity in the southern hemisphere is generally higher and more homogenous in the Miocene (cf. Figures 3a and 3b). A positive salinity anomaly in Southeast Asia in the Miocene case is attributed to the removal of Borneo and its associated continental runoff in the Miocene geography (Figure 3c). The Miocene tropics are generally more saline than in our modern case. Tethys throughflow is westward with salinities between 34–36‰, though drop to as low as 16‰ in the Lago-Mare due to continental runoff (Figure 3b). The far North Atlantic is considerably fresher in the Miocene which is likely due to a fresher East Greenland Current compared to the modern (cf. Figures 3a and 3b) and to a lesser extent an open Panama gateway [*Lunt et al.*, 2008; *Maier-Reimer et al.*, 1990]. The East Greenland Current is in turn fed by a significantly fresher Arctic, with Miocene salinities between 21–23‰ compared to modern salinities of 28–30‰. The Miocene Arctic is characterized by a relatively thick halocline consistent with high concentrations of freshwater algae [*Sangiorgi et al.*, 2008]. This salinity decrease is attributed to significantly higher river runoff from circum-Arctic landmasses (not shown). In our Miocene simulation, approximately 7,124 km^3/yr of fresh

Figure 2. Mixed-layer temperature and velocity fields (cm/s) for the (a) modern and (b) Miocene cases. (c) Miocene minus modern case anomaly. The control and Miocene cases are calculated on different grids. To calculate Figure 2c, the control case temperature field is interpolated to the Miocene grid and consequently continental outlines differ in some regions. Velocity reference lengths are 15 cm/s (Figures 2a and 2b) and 5 cm/s (Figure 2c).

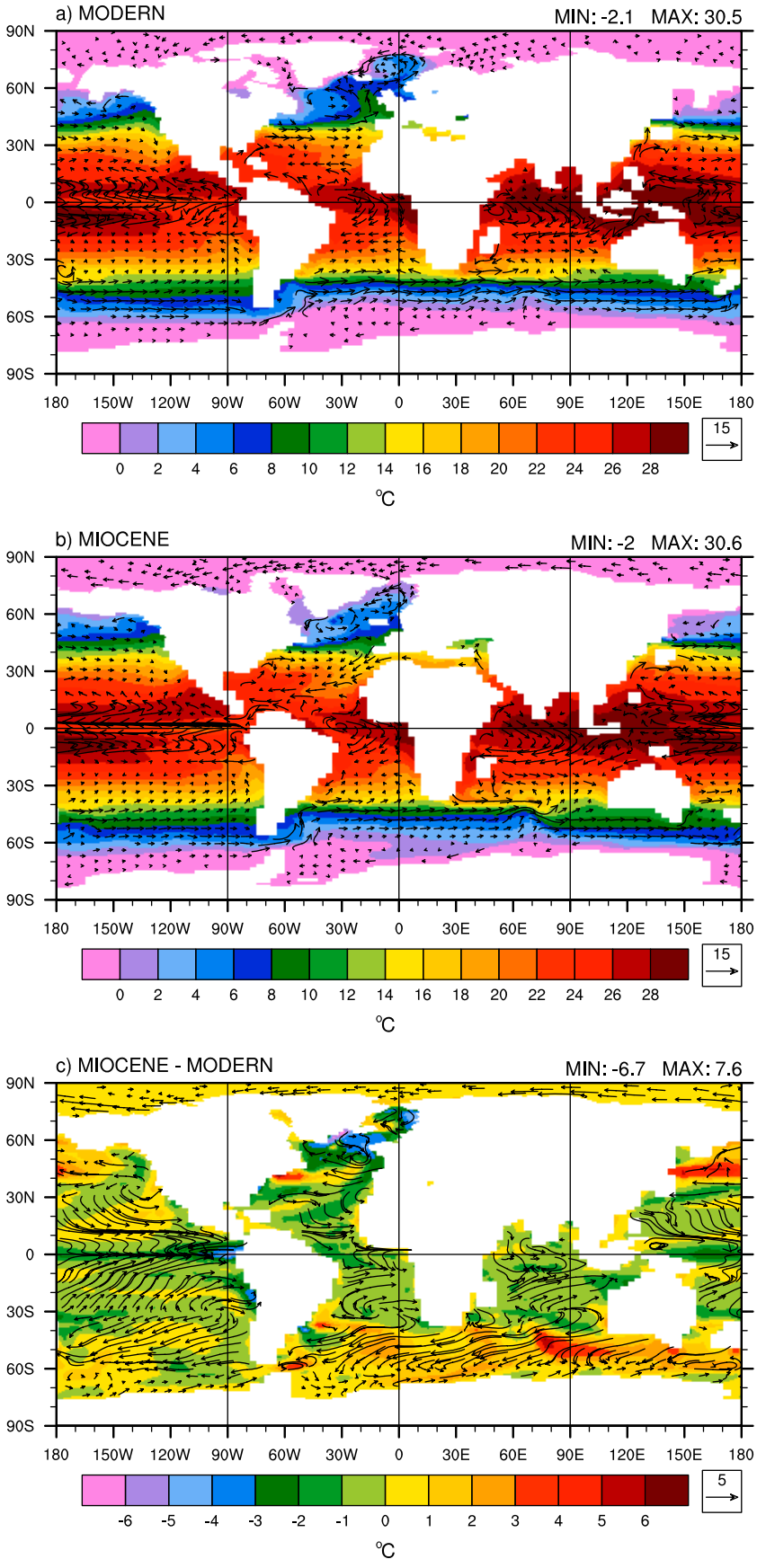
a) MODERN
MIN: -2.1 MAX: 30.5
b) MIOCENE
MIN: -2 MAX: 30.6
c) MIOCENE - MODERN
MIN: -6.7 MAX: 7.6
90N
60N
30N
0
30S
60S
90S
180 150W 120W 90W 60W 30W 0 30E 60E 90E 120E 150E 180
0 2 4 6 8 10 12 14 16 18 20 22 24 26 28
15
°C
-6 -5 -4 -3 -2 -1 0 1 2 3 4 5 6
5

Figure 2

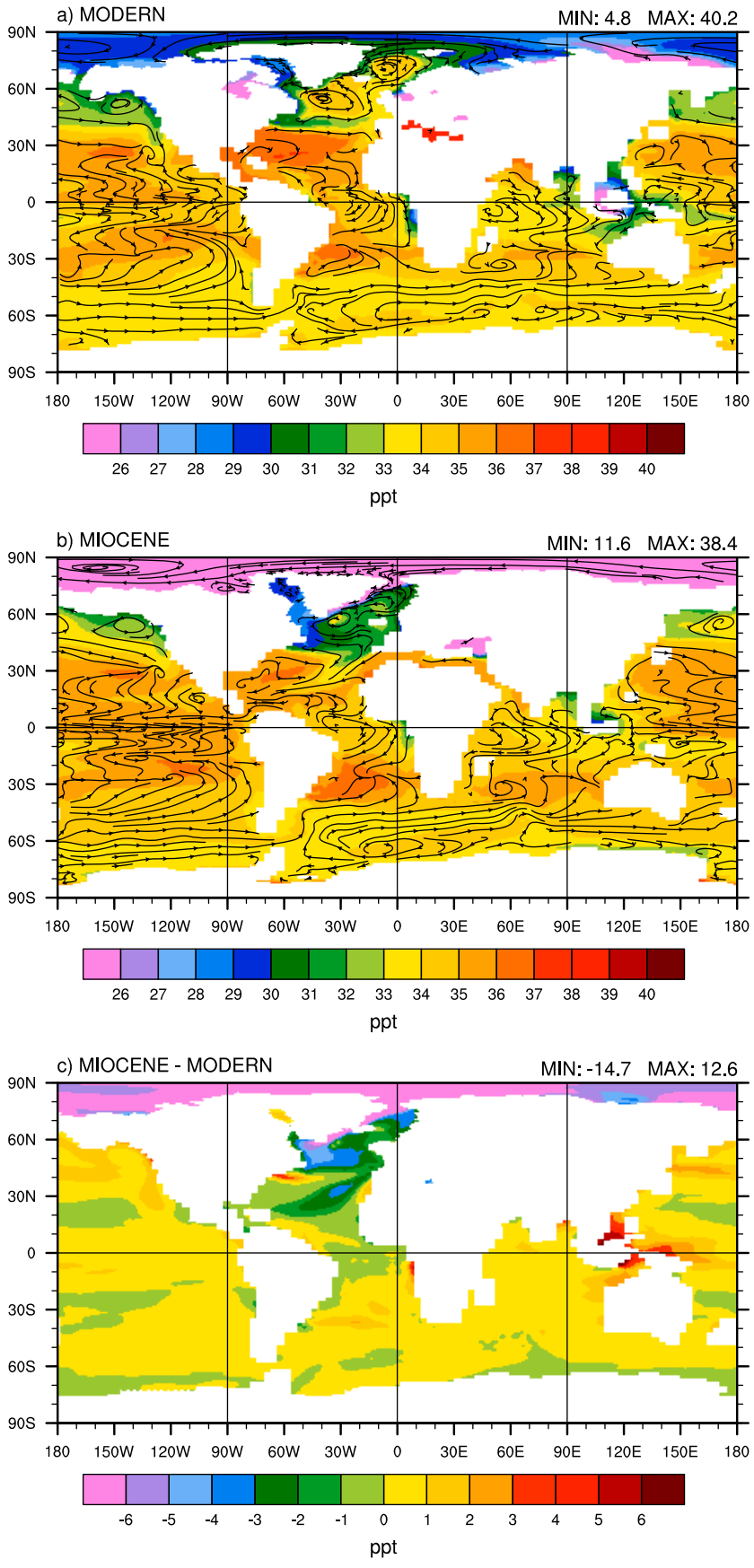

Figure 3. Same as Figure 2 except for salinity. Streamlines shown in Figures 3a and 3b.

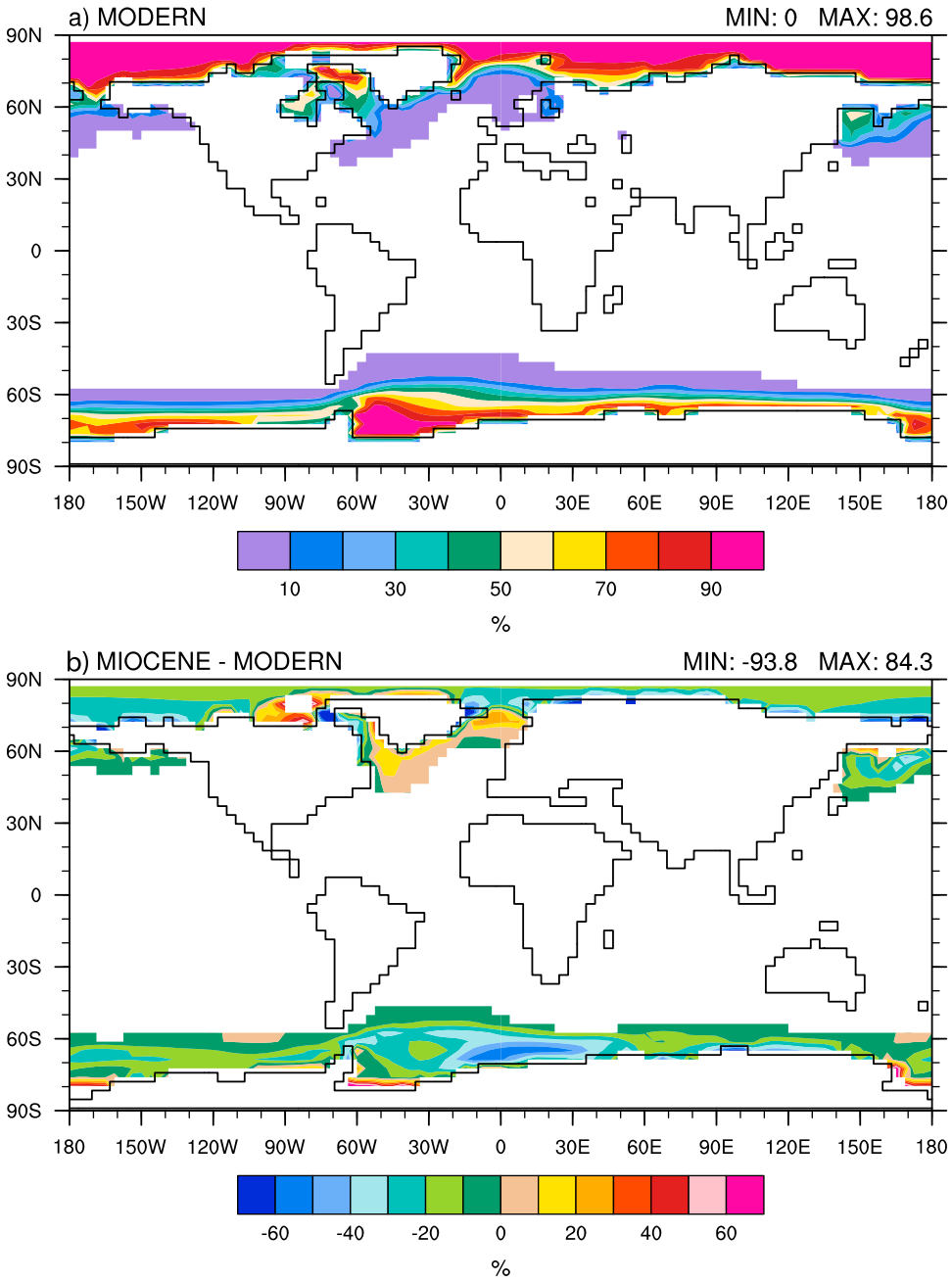

Figure 4. Mean annual sea-ice concentration for (a) the modern case and (b) the Miocene minus modern anomaly.

water enters the Arctic Ocean via river runoff, compared to 3,709 km^3/yr in the modern simulation. This is due in part to precipitation over the area of the modern Hudson Bay and Barents Sea, which are land in the Miocene (Figure 1), being transported to the Arctic Ocean in our Miocene simulation. A stronger Miocene hydrological cycle compared to the modern, defined by an approximately 1,248 km^3/yr increase in net precipitation (precipitation minus evaporation) poleward of 60°N, also plays a significant role. Uncertainty in river runoff to the Arctic exists as river direction in our Miocene simulation is dictated only by topographic relief, which alone is not necessarily a realistic indicator of flow (see *Bice et al.* [1997] for a sensitivity analysis). The lack of relatively saline flow through the Fram and Bering Straits (Figure 3a) would also contribute to sea-surface freshening in the Miocene Arctic. Similarly, North Pacific salinity is higher in the Miocene due to lower river runoff. Surface flow through the Fram Strait is southward in the Miocene, similar to but weaker than the modern case (Figure 3b). The Miocene transpolar drift flows along the entire Arctic coastline in contrast to the modern, characterizing a 'circum Arctic' drift and compressing the Beaufort Gyre (Figure 3b).

4.2. Sea-Ice Extent

[10] In the northern hemisphere, modeled annual sea-ice concentrations are significantly lower in the Miocene over

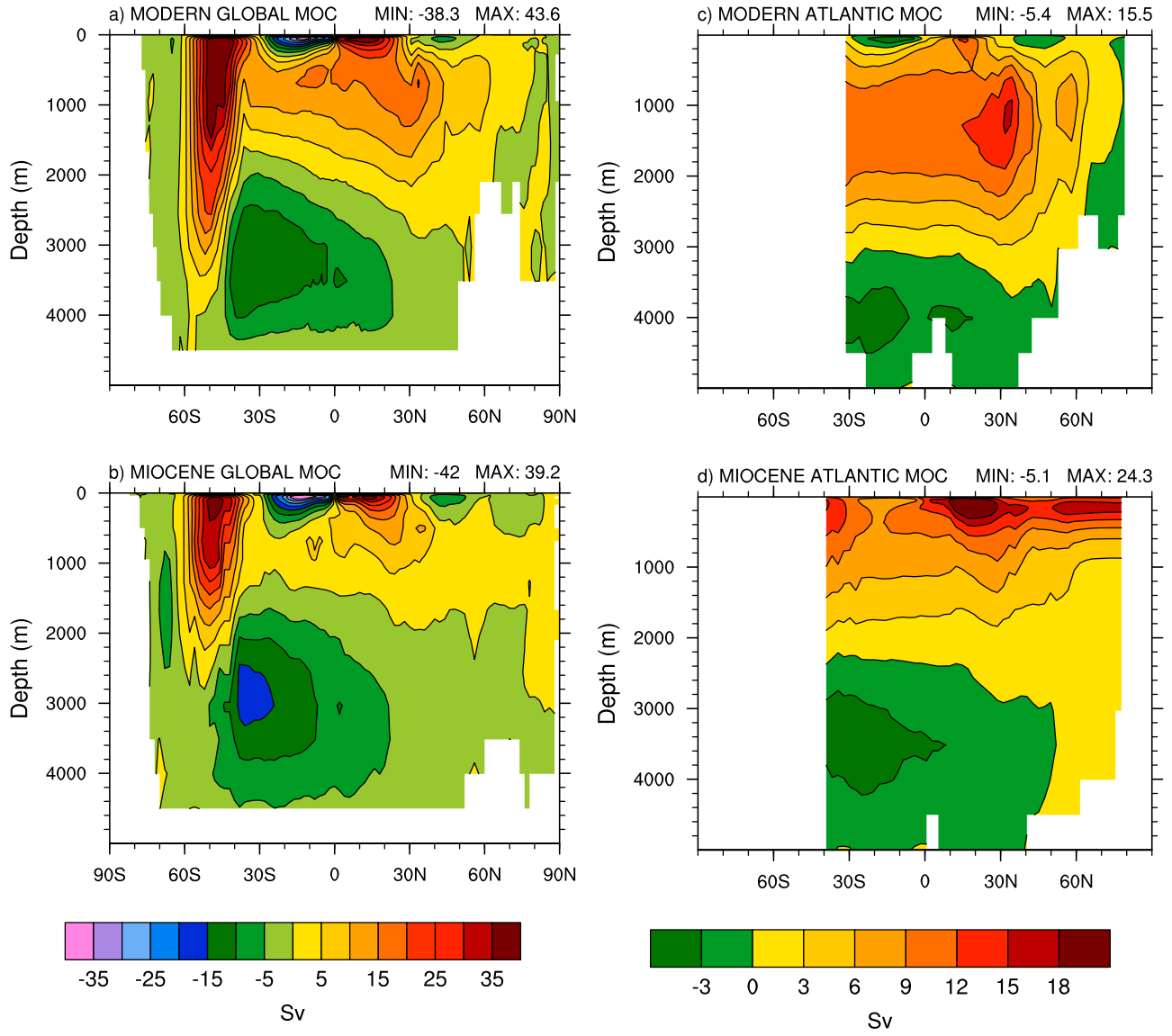

Figure 5. (a, b) Eulerian global and (c, d) Atlantic meridional overturning circulation (MOC) for the modern and Miocene cases.

large parts of the Arctic and far North Pacific Oceans (Figure 4). Conversely, concentrations increase in the Miocene North Atlantic due to cooler mixed-layer temperatures associated with weaker North Atlantic Deep Water formation (Figure 2c). In the southern hemisphere there is a clear reduction of sea-ice in the Miocene east of the Weddell Sea, where substantial bottom water formation is simulated (see section 4.4). Consequently, the majority of this reduction occurs during southern hemisphere winter. Northern hemisphere annual sea-ice area is 7.5×10^6 km^2 in the Miocene simulation compared to 13.3×10^6 km^2 in the modern. However, a large part of this is due to the increased surface area of Europe and North America in the Miocene, at the expense of ocean area (Figure 1). In the southern hemisphere, annual sea-ice area is 8.5×10^6 km^2 in the Miocene and 13.1×10^6 km^2 in the modern.

[11] Sea-ice proxy records are qualitative however ice-rafting debris suggest Arctic sea-ice production was modest between 17.5 and 16 Ma and more prevalent prior to and following this interval [*St. John*, 2008]. Extremely warm, shallow water sea-surface temperatures (SSTs; 23.5°C) in the far North Pacific—though only intermittently this warm [*Oleinik et al.*, 2008]—are consistent with minimal sea-ice during the early to middle Miocene. Furthermore, several studies suggest perennial sea-ice in the northern hemisphere initiated subsequent to the Miocene climatic optimum [*Backman and Moran*, 2009, and references therein]. Thus there is likely excessive sea-ice in our Miocene simulation.

4.3. Meridional Overturning Circulation and Gyre Transport

[12] Global meridional overturning circulation is considerably weaker in the Miocene. The Deacon cell is relatively sluggish and persists to a depth of 2,800 m, compared to 4,000 m in the modern case (Figures 5a and 5b). In the Miocene, northward flow of Antarctic bottom water is more

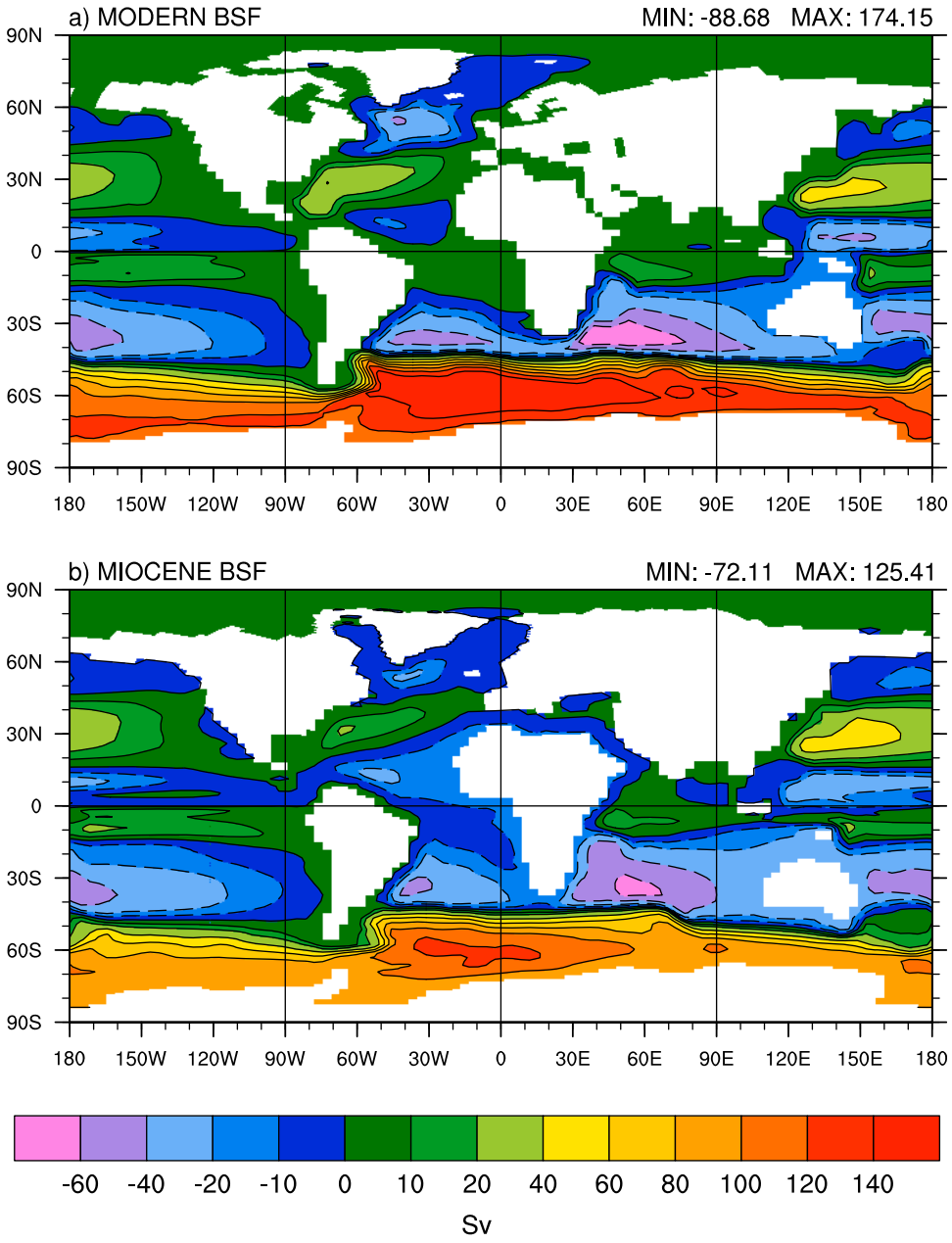

Figure 6. Barotropic stream function for the (a) modern and (b) Miocene cases.

intense and pervasive compared to the modern. The low resolution version of the CCSM3 reproduces modern North Atlantic overturning rates toward the lower end of observed values [*Yeager et al.*, 2006]. NADW formation in the Miocene is weaker than simulated for the modern and is restricted to the upper 1,500 m. This overturning is extended into the far North Atlantic (>60°N) by a shallow, intense circulation facilitated by the near-absence of the GSR (Greenland-Scotland Ridge) (Figures 5c and 5d), however, this does not reflect deep water formation. As Figure 5 represents the eularian component of the overturning circulation, a more appropriate indication of tracer transport is given by ideal-age and is discussed in the next section.

[13] Gyre circulation is also less vigorous in the Miocene, particularly in the North Atlantic Ocean (Figure 6). The largest difference between cases is the connection of the South Pacific and Indian Ocean gyres in the Miocene due to the wider Indonesian gateway. The South Atlantic and Indian Ocean gyres are weaker in the Miocene and exchange between the two oceans is reduced. This is associated with a weakening of the midlatitude westerlies and the slight southerly position of Africa in the Miocene. Simulated volume transport by the Antarctic Circumpolar Current is up to 92 Sv in the Miocene, compared to 105 Sv in the modern case (Table 1).

[14] The weaker Miocene ocean circulation compared to the modern is attributed in part to a reduced meridional surface temperature gradient and consequent weakening of the southern hemisphere midlatitude westerlies (Figure 7). Substantial reductions in wind stress curl and barotropic

Table 1. Volume Transport Through Gateways in Sv[a]

Gateway	Modern	Miocene	HiCO2
Drake (zonal)	105	92	88
Fram (meridional)	−0.33	1.068×10^{-4}	-1.5×10^{-4}
Bering (meridional)	0.37	N/A	N/A
Baffin Bay (meridional)	−0.89	N/A	N/A
Barents Sea (zonal)	0.85	N/A	N/A
Panama (zonal)	N/A	0.64	0.56
Tethys (zonal)	N/A	−11.3	−11.5

[a]Parentheses indicate orientation of throughflow. For zonal throughflow, positive values indicate eastward flow and negative values indicate westward flow. For meridional throughflow, positive values indicate northward flow and negative values indicate southward flow.

stream function arise because of the reduction of these winds. Weakening of the North Atlantic subtropical gyre may be attributed in part to the open Panama gateway, which model sensitivity tests have shown to weaken the western boundary current [*Maier-Reimer et al.*, 1990], however, reduced sea level pressure gradients and the associated weakening of surface winds (Figure 8) are likely the dominant forcing. Regional influences at sites of convection also influence the overturning circulation.

4.4. Water Mass Formation

[15] The formation of intermediate and bottom water masses and their subsequent trajectories are diagnosed using the 'ideal age' tracer, maximum winter boundary layer depths and velocity fields. Ideal age represents the number

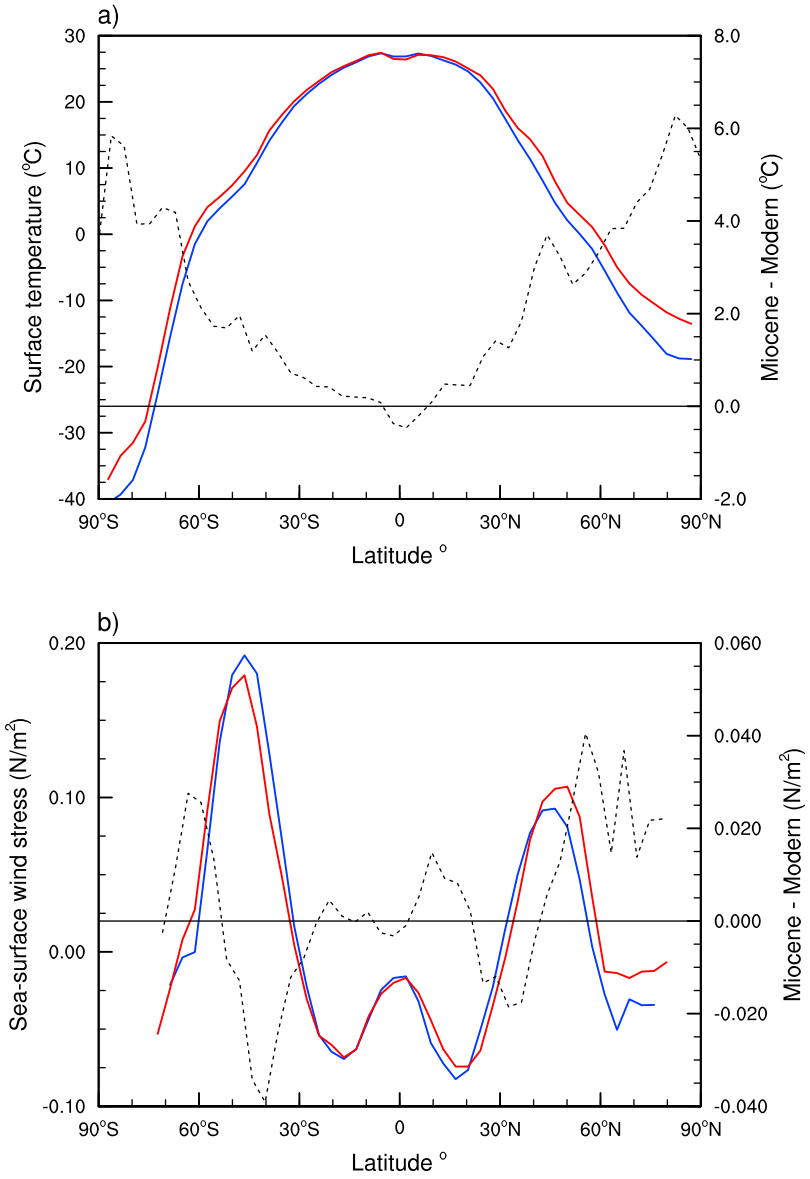

Figure 7. (a) Zonal annual mean surface temperature and (b) sea-surface wind stress for the modern (blue) and Miocene cases (red). Dashed lines are Miocene minus modern anomalies with reference to right *y* axis.

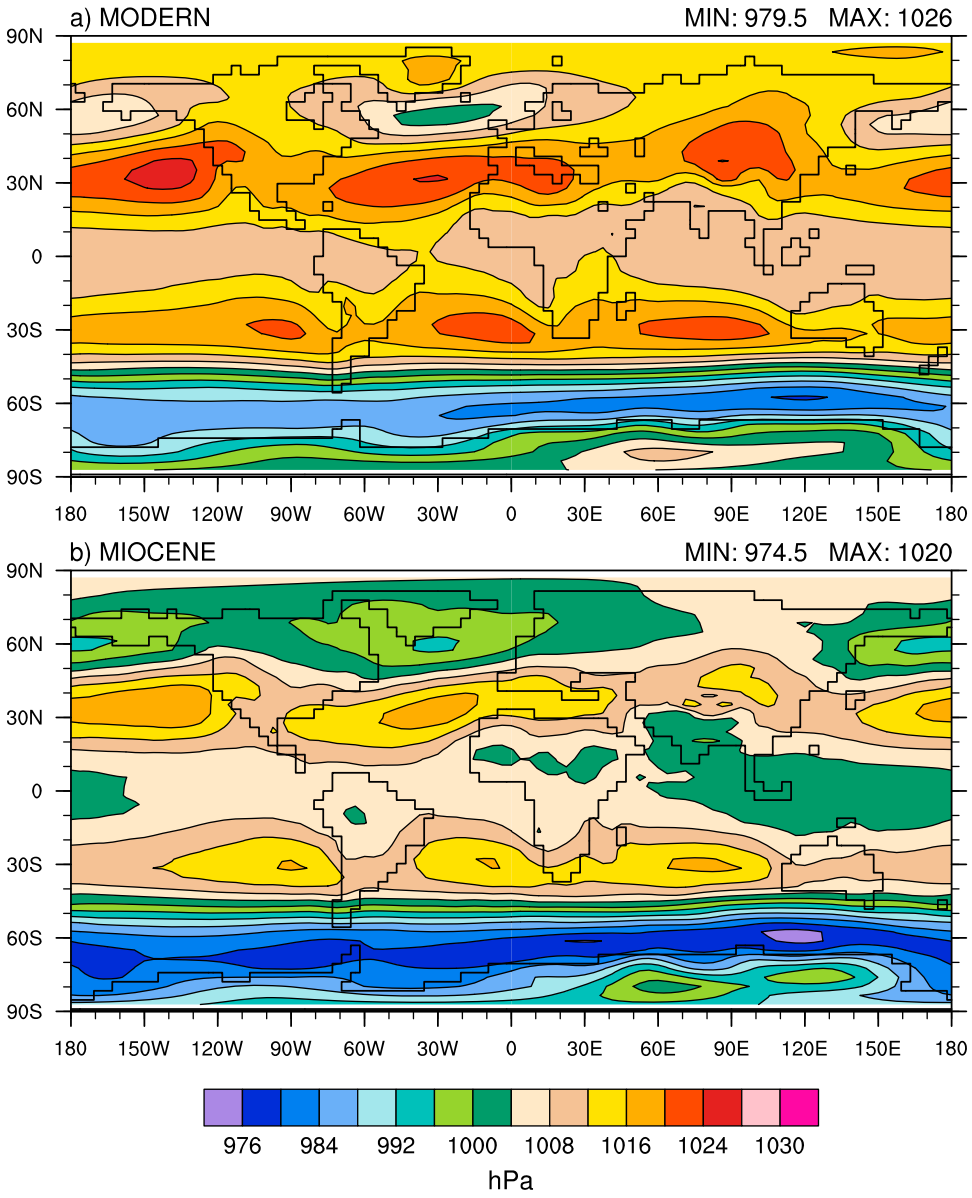

Figure 8. Mean annual sea level pressure for the (a) modern and (b) Miocene cases.

of years water has been isolated from the sea-surface. The most significant changes between the control and Miocene cases occur in the Atlantic and thus we focus our discussion here. In the Miocene southern hemisphere significant bottom water formation is simulated in the Weddell Sea with weaker formation in the vicinity of the Ross Sea and Marie Byrd Land coast, consistent with an inferred dominant deep water source in the Southern Ocean [*Wright and Miller*, 1993]. Initial sinking of Weddell Sea bottom water occurs to the east, indicated by a pronounced deepening of the winter boundary layer (Figure 9b). After descending to 4,000 m Weddell Sea bottom water flows west along the Pacific-Antarctic ridge before turning north and east into the South Pacific and Indian Ocean basins. Accordingly bottom waters in the Pacific and Atlantic basins age northward, consistent with carbon isotope interpretations [*Woodruff and Savin*, 1989]. This scenario differs from the modern case where bottom water forms only weakly along the Ross Sea and Marie Byrd Land coast. This is discussed further in section 5.1.

[16] Formation of proto-NADW in the Miocene (hereafter referred to as North Component Water; NCW) is simulated in the Labrador Sea; however, it is significantly weaker than its modern counterpart (Figure 10). Maximum winter boundary layer depth in the far North Atlantic is 150 m in the Miocene compared to 650 m in the modern (Figure 9). NCW descends to approximately 1,500 m, compared to approximately 3,000 m for NADW (Figure 10). No deep water formation is simulated in the Greenland-Norwegian Seas in the Miocene (Figure 9).

[17] NCW is significantly warmer and more saline than NADW (Figure 11), resulting in an overall lower density. The mixed-layer in the Labrador Sea and off southeast

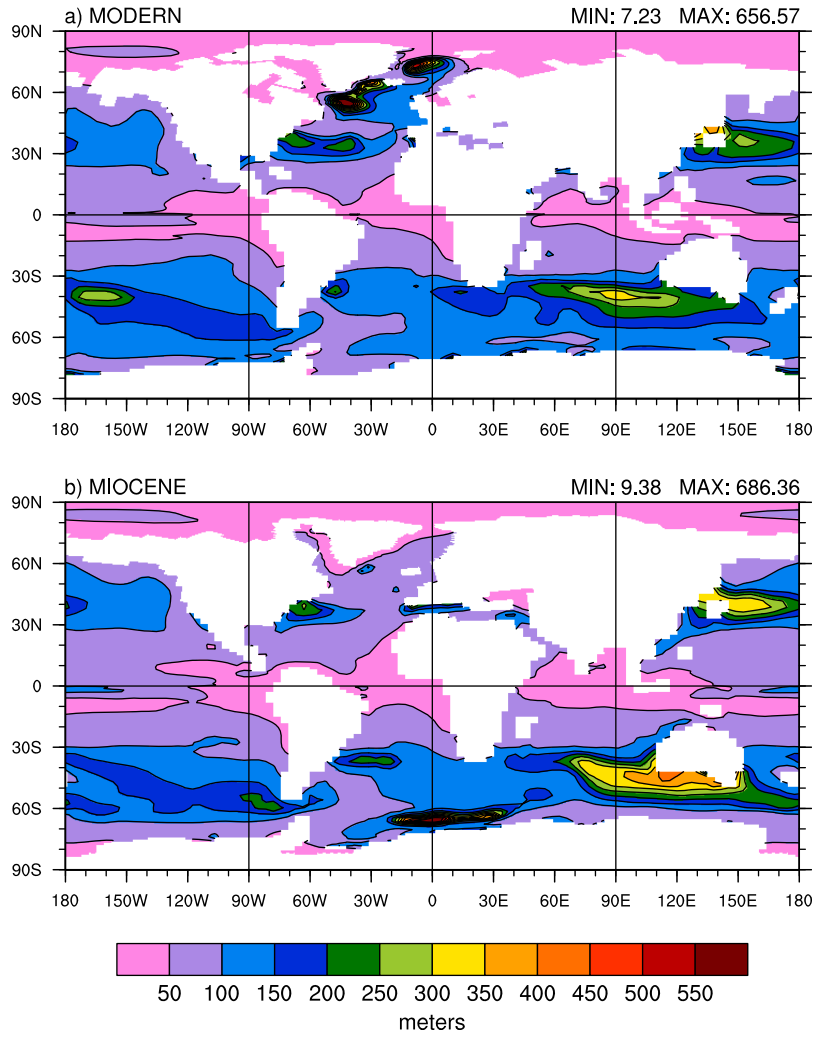

Figure 9. Winter time maximum boundary layer depth for the (a) modern and (b) Miocene cases.

Greenland—where NADW forms in the modern case (Figure 9a)—is significantly fresher in the Miocene, contributing to the meager convection. This in turn can be explained by the relatively fresh East Greenland Current (Figure 3). Interestingly, temperature and salinity of NCW increases considerably below the mixed-layer. This is a result of exported subtropical water below the mixed-layer and is attributed to several factors. First, the Miocene subtropical gyre extends further northeastward compared to the control case (Figure 6) in association with a shift in the subtropical high pressure cell (Figure 8). We note this circulation brings Tethys outflow across the tropical North Atlantic to the Panama gateway (Figure 2b). Second, a weakening of the subpolar gyre leads to greater entrainment of northward flowing subtropical waters (Figure 6), warming the western side of the basin and NCW in the process, consistent with modern observations [*Bindoff et al.*, 2007, pp. 396–397]. In our Miocene case this weakening is attributed to the almost absent anti-cyclonic circulation over Greenland due to a lower elevation and albedo compared to the modern (Figure 8). While subtropical water flows into the far North Atlantic in our modern simulation, mixing with the relatively stronger subpolar gyre is minimal. Finally, the reduced deep water formation in our Miocene case reduces vertical mixing of relatively cool surface waters. Consequently, a large temperature inversion exists in the Miocene far North Atlantic compared to the modern.

[18] In the Miocene case, subtropical water below the mixed-layer also enters the Greenland-Norwegian Seas and Arctic basin, along the eastern boundary. The deepest section of the GSR, which separates the Greenland-Norwegian Seas from the rest of the North Atlantic, is 4,000 m in our Miocene case and 950 m in our modern case (Figure 1). This fundamental change in circulation results in Miocene temperatures 4–5°C higher in the Greenland-Norwegian Seas and Arctic basin compared to the modern (Figure 11a), a result consistent with sensitivity tests of GSR bathymetry [*Robinson et al.*, 2011].

[19] At approximately 1,500 m depth, NCW flows equatorward and is joined by a weak eastward Panama throughflow before continuing south as a western boundary current and mixing with the South Atlantic subtropical gyre (Figure 12). Similar southward flow occurs in the modern case however this originates from the North Atlantic subtropical gyre, which is nearly unidentifiable in the Miocene (Figure 12). Flow patterns from the tropical North Atlantic

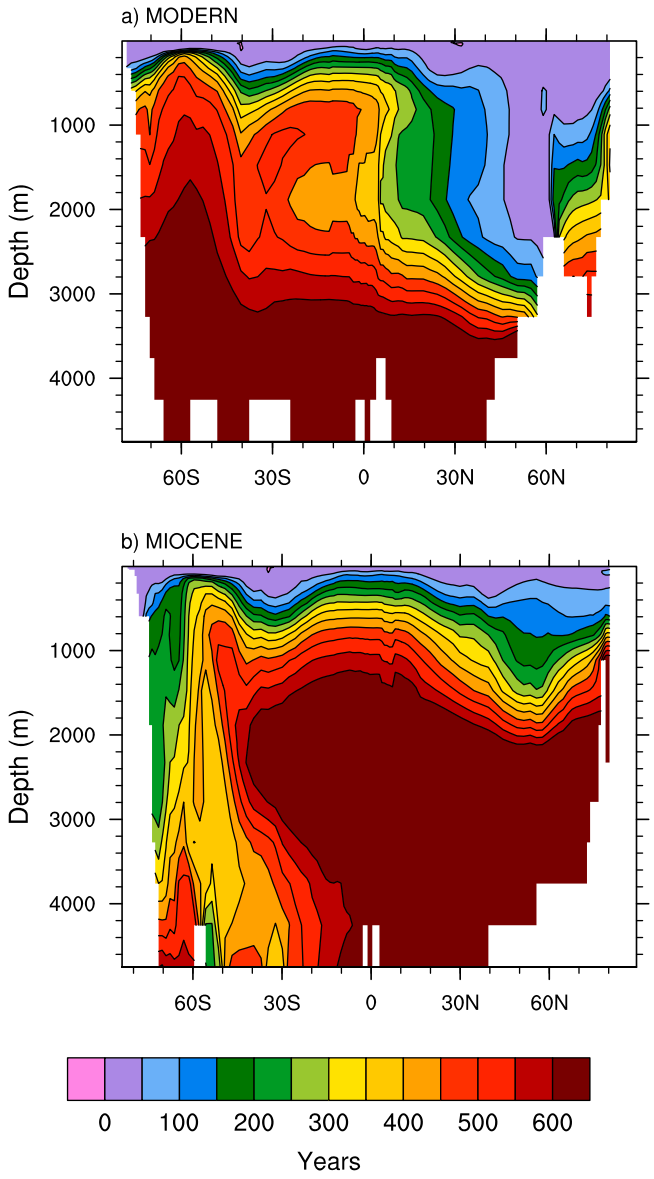

Figure 10. Zonal mean Atlantic basin ideal age for the (a) modern and (b) Miocene cases.

to the South Atlantic are similar between the modern and Miocene cases between 1,000 and 1,500 m, above this the modern circulation shows a reversal of the boundary current in the western tropical Atlantic (to a northwesterly direction). Between 1,500 and 3,000 m, flow patterns change little in both simulations, except that velocities decrease significantly with depth in the Miocene and outflow from the Labrador Sea in the modern case starts to occur below 2,000 m. Modeled South Atlantic temperatures in the Miocene are 1–4°C above present between 300–1,500 m (Figure 11a). This relative warmth is attributed to entrainment of NCW by the South Atlantic gyre. As NCW does not descend as deeply as NADW, its southward flow does not reach the Southern Ocean.

[20] The depth of the Fram Strait is 2,100 m and 1,300 m in our modern and Miocene cases respectively. Flow structure through the Fram Strait in our Miocene case is consistent with reconstructed sea-ice migration patterns subsequent to the Miocene climatic optimum [*Knies and Gaina*, 2008] and is similar to the transient 'enclosed estuarine sea' regime proposed to have occurred during gateway widening [*Jakobsson et al.*, 2007]. Net volume transport through the Fram Strait is southward in the modern case (−0.33 Sv) and is balanced by flow through the Barents Sea, Bering Strait and Davis Strait (Table 1). In the Miocene case the Fram Strait is the only gateway into the Arctic basin and thus exhibits negligible net transport.

4.5. Meridional Heat Transport

[21] Global ocean heat transport differs significantly in the Miocene case, with a near-symmetrical distribution about the equator (Figure 13). Peak global ocean heat transport in the Miocene southern hemisphere is up to 0.7 PW greater than modern. While temperatures in the far North Atlantic

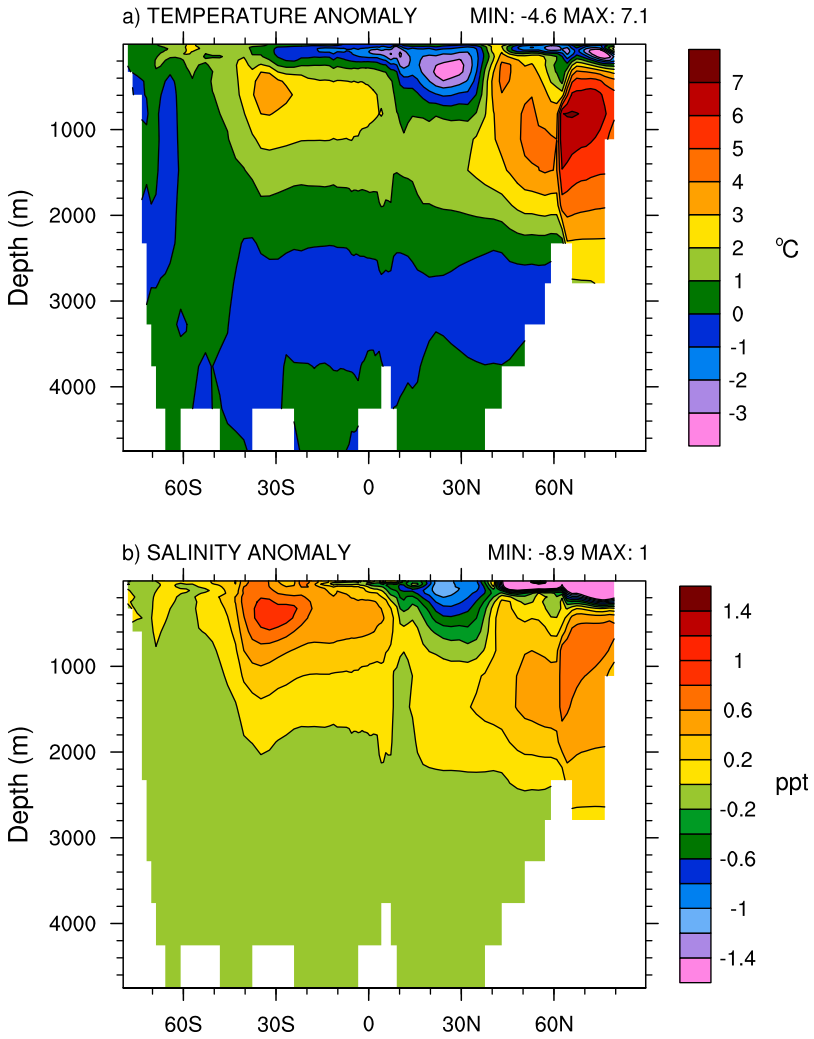

Figure 11. Miocene minus modern (a) temperature and (b) salinity anomalies for the Atlantic basin.

below the mixed-layer are significantly warmer in the Miocene case (Figure 11a) this heat is not transferred to the atmosphere, thus Miocene ocean heat transport in the far North Atlantic is less than half that of the modern (Figure 13). The majority of global heat transport change is attributable to the weakening of deep water formation in the North Atlantic and the associated disruption in 'heat piracy' from the southern hemisphere into the northern hemisphere. From the high northern latitudes to middle southern latitudes, changes in Atlantic heat transport are nearly directly translated onto the global heat transport budget. However, poleward of 45°S the large southward increase in Atlantic heat transport in the Miocene is compensated by a decrease in southward heat transport in the Indian Ocean (Figure 13). A shallower-than-modern Kerguelen Plateau leads to enhanced topographic steering of the Antarctic Circumpolar Current in the Miocene and a poleward shift of the sub-Antarctic front. The effects of this can be clearly seen in the positive temperature anomaly in Figure 2c at approximately 75°E and 45°S. The near-constancy of zonal mean heat transport poleward of 45°S is a robust feature in coupled paleoclimate modeling studies [*Huber and Nof*, 2006; *Huber et al.*, 2004].

4.6. Benthic Temperature Comparison

[22] Estimates of SST from planktonic foraminifera are subject to various uncertainties including assumptions of paleo-current distributions and until recently have suffered poor quality control over early diagenesis (the reader is referred to *Crowley and Zachos* [2000] for uncertainties regarding oxygen isotope paleothermometry). Too few well-preserved planktonic foraminifer assemblages have been analyzed to date to make a useful comparison with modeled SSTs. Conversely, benthic foraminifera assemblages are significantly less affected by diagenesis and uncertainties in deep water pathways. Therefore we utilize published deep water temperature estimates in our model-data analysis (Table 2 and Figure 1).

[23] As direct model-data comparisons do not take into account model bias we compare the warming between modern day observations and proxy records with the warming simulated between our Miocene and modern cases. The mean warming between our Miocene and modern cases across all proxy localities is 0.3°C, compared to a 4.7°C warming between proxy records and modern observations (Table 2). Thus sites of bottom water formation in our

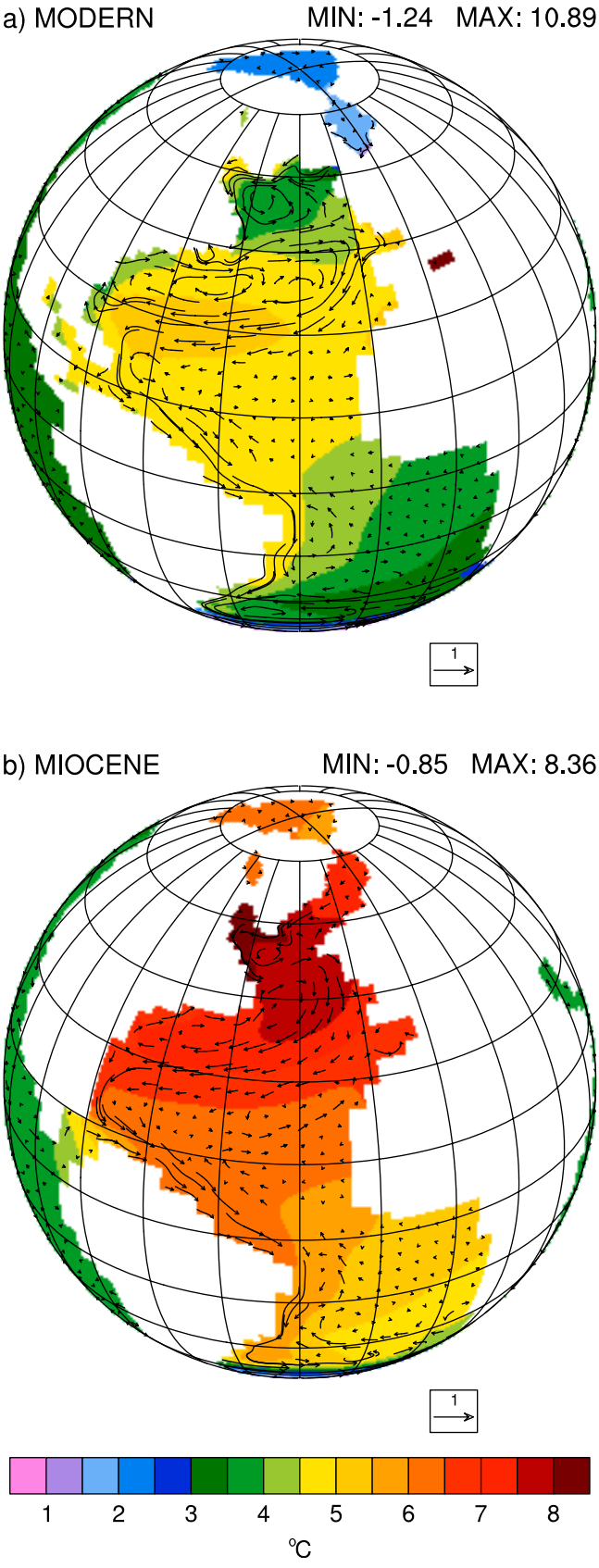

Figure 12. Temperature and velocity fields at 1,500 m depth for the (a) modern and (b) Miocene cases. Velocity reference length is 1 cm/s.

Miocene case are significantly cooler than suggested by proxy records. This is somewhat expected considering that high latitude SSTs are cool enough to maintain considerable sea-ice formation in our Miocene case and that ice formation, the associated brine rejection and thus presumably deep water formation occur at similar temperatures compared to the present. Miocene deep water warming of the magnitude suggested by proxy records (Table 2) could only be produced by either high latitude SSTs above 0°C (either zonally or locally at sites of deep convection) or a dominant low latitude bottom water source. However, we note the cold bias in our model is overestimated by the fact that the control case is equilibrated to 'modern' (1990) greenhouse gases, whereas observations represent the transient response to antecedent increases in greenhouse gases. Though we speculate this has only a minor effect.

[24] A direct comparison of temperatures between our modern case and modern observations reveals a mean cold bias of −0.3°C (compare modern case temperature and modern observed temperature columns in Table 2), compared to −3.5°C between our Miocene case and proxy records. This might suggest that the overwhelming majority of the model-data discrepancy is due to our Miocene boundary conditions and/or proxy records. However, it is difficult to imagine what boundary condition could produce the changes necessary to reconcile these model-data discrepancies (with the exception of CO_2, see next section). The diverse range of independently formulated marine and terrestrial proxy data available in the literature also suggests with near-unanimity a globally warmer climate. Thus there are likely significant weaknesses in the sensitivity of the CCSM3, this is consistent with growing evidence that current generation GCMs, while simulating modern climates with considerable competence, are insufficiently sensitive to large magnitude climate forcings [*Huber and Caballero*, 2011; *Valdes*, 2011].

4.7. CO_2 Sensitivity

[25] While CO_2 proxies have converged over the past decade Miocene estimates still vary by more than a factor of two [*Beerling and Royer*, 2011]. Given the potentially large influence of CO_2 on ocean circulation an additional Miocene simulation is conducted with a CO_2 concentration of 560 ppmv, twice that of the pre-industrial era. This simulation (referred to as the HiCO2 case) is branched from the standard Miocene simulation and run for 900 years to equilibrium, based on volume integrated ocean temperature. The last 100 years of output are used for analysis. Compared to the standard Miocene case, a strengthening of southern hemisphere bottom water formation, particularly in the Weddell Sea, is simulated (cf. Figures 10b and 14a). Conversely, a weakening of NCW formation occurs, with the 600 year ideal age contour approximately 300 m shallower than in the standard Miocene case. Given that the low resolution CCSM3 has a lower climate sensitivity compared with higher resolution versions of the model [*Otto-Bliesner et al.*, 2006] and that some Miocene CO_2 reconstructions are higher than 560 ppmv [*Kürschner et al.*, 2008], higher Miocene CO_2 conditions could have significantly weakened or even terminated NCW formation in our model, as has been suggested for most of the early Miocene [*Woodruff and Savin*, 1989].

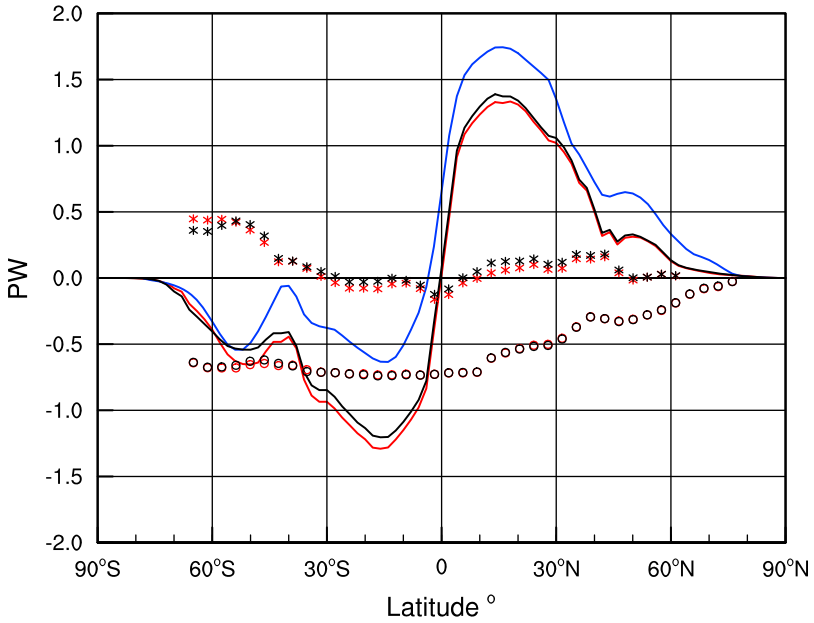

Figure 13. Global ocean heat transport for the Miocene (red), modern (blue) and HiCO2 cases (black; see section 4.7) shown with solid lines. Miocene minus modern ocean heat transport anomalies for the Atlantic (red circles) and Indian + Pacific Oceans (red asterisks). HiCO2 minus modern ocean heat transport anomalies for the Atlantic (black circles) and Indian + Pacific Oceans (black asterisks).

[26] Ocean heat transport changes in the HiCO2 case are small and occur mostly in the southern hemisphere (Figure 13). A warming of approximately 1°C occurs throughout most of the Atlantic Ocean to a depth of 500 m, though a distinct cooling in the North Atlantic occurs between 500 and 1,000 m due to reduced NCW outflow (Figure 14b). In the Arctic, temperatures warm by 1°C at 1,000 m depth to over 2°C at the deepest level. Patterns of global zonal temperature change between the HiCO2 and standard Miocene cases are similar to the Atlantic temperature anomaly shown in Figure 14b, in that the majority of warming occurs above 1,000 m, with the exception of the

Table 2. Temperature Change Simulated by the CCSM3 Versus Temperature Change Between Modern Observations and Proxy Records[a]

Location	Paleo Depth[b] (m)	Paleo Longitude/Latitude[c]	Modern Case Temperature (°C)	Miocene Case Temperature (°C)	HiCO2 Case Temperature (°C)	Simulated Warming Miocene Case[d] (°C)	Simulated Warming HiCO2 Case[e] (°C)	Modern Observed Temperature[f] (°C)	Miocene Proxy Temperature[g] (°C)	Proxy Derived Warming[h] (°C)	Reference[i]
DSDP15	4660	−18.5/−29.9	1.0	0.9	0.9	−0.2	−0.2	2.0	6.9	4.9	1
DSDP22	2230	−31.4/−31.3	3.3	3.4	3.4	0.1	0.1	2.8	6.9	4.1	1
DSDP55	3180	153.9/7.6	1.4	1.9	2.3	0.5	0.8	1.9	6.9	5.0	1
DSDP167	2910	195.7/3.4	1.8	2.3	2.7	0.5	0.9	1.6	6.9	5.3	1
DSDP279	3980	169.5/−53.3	1.1	1.4	1.7	0.4	0.6	1.3	6.9	5.6	2
ODP747A	1640	75.9/−52.2	1.3	1.7	2.3	0.5	1.0	2.1	7.5	5.4	3
ODP1171	1980	148.9/−54.4	2.5	2.6	2.9	0.1	0.3	3.0	6	3.0	4
DSDP573	4390	−121.9/−3.4	1.0	1.7	2.0	0.7	0.9	1.4	6	4.6	5
Mean						0.3	0.6			4.7	

[a]To facilitate comparison between model cases and observations/proxy records, model temperatures are converted from potential to in situ temperatures based on *Fofonoff and Millard* [1983].
[b]Paleo depths calculated by adjusting for sediment load and compaction since sample deposition and by calculating subsidence since sample deposition using the GDH-1 model of *Stein and Stein* [1992].
[c]Where paleo coordinates are not provided by reference, values are calculated using modern coordinates, a plate kinematic model and the rotations of *Müller et al.* [2008].
[d]Miocene minus modern case temperature.
[e]HiCO2 minus modern case temperature.
[f]Levitus 1994 World Ocean Atlas (NODC_WOA94 data provided by the NOAA/OAR/ESRL PSD, Boulder, Colorado, USA, from their Web site at http://www.esrl.noaa.gov/psd/).
[g]Where a range of values is given, the mean is used.
[h]Miocene proxy temperature minus modern observed temperature.
[i]References: (1) *Savin et al.* [1975], (2) *Shackleton and Kennett* [1975], (3) *Billups and Schrag* [2002], (4) *Shevenell et al.* [2008], and (5) *Lear et al.* [2000].

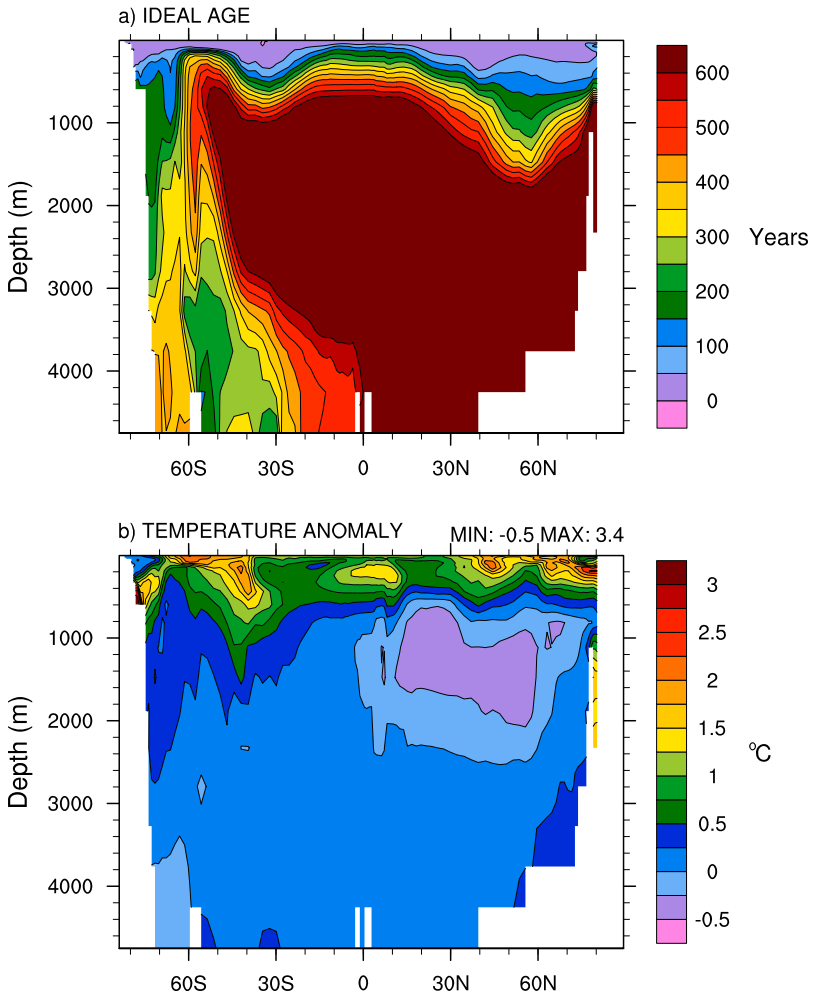

Figure 14. (a) Ideal age for the HiCO2 case and (b) the HiCO2 minus Miocene temperature anomaly for the Atlantic basin.

Arctic which warms increasingly with depth. Consequently, the simulated mean warming at proxy drill locations between HiCO2 and our modern case increases only slightly (by 0.3°C; Table 2) and is still significantly less than the warming indicated by proxies. Global surface temperature in the HiCO2 case is 1.6°C warmer than the standard Miocene simulation, with maximum surface radiative warming over the Weddell Sea due to significant sea-ice reduction associated with stronger bottom water formation. Northern hemisphere annual sea-ice area decreases from 7.5×10^6 km^2 in the standard Miocene case to 5.7×10^6 km^2 in the HiCO2 case. In the southern hemisphere, sea-ice area decreases from 8.5×10^6 km^2 to 5.5×10^6 km^2. Similar to the sea-ice anomaly pattern between the standard Miocene case and the modern (Figure 4), the majority of sea-ice decrease in the HiCO2 case compared to the standard Miocene case occurs in the Weddell Sea (not shown).

5. Discussion

5.1. Deep Water Circulation

[27] Our model results show fundamental circulation differences between the Miocene and modern oceans. The moderate formation of NCW in our Miocene case relative to the present is qualitatively consistent with previous ocean models [*Barron and Peterson*, 1991; *Bice et al.*, 2000; *von der Heydt and Dijkstra*, 2006] and various tracer data [*Via and Thomas*, 2006; *Wright et al.*, 1992], though some interpretations suggest that this may be more representative of the late Miocene [*Woodruff and Savin*, 1989]. Conversely, *Wright et al.* [1992, Figures 13 and 14] infer the existence of NCW formation to depths of 3,500 m, compared to 1,500 m in our Miocene case (Figure 10). The subsequent path of NCW is also at odds with previous modeling. *Nisancioglu et al.* [2003] performed a series of Miocene ocean general circulation model experiments to test the sensitivity of Panama throughflow to varying sill depths. While their experiments are idealized, they show that a Panama sill depth greater than NCW outflow from the North Atlantic should drive NCW from the Atlantic to the Pacific, with an eastward surface flow. Outflow of NCW from the North Atlantic in our Miocene case occurs from approximately 1,000 m to 2,000 m and the depth of the deepest path to the Panama gateway is 1,700 m, however flow through the gateway between the mixed-layer and this depth is eastward. NCW in our Miocene case instead enters the South Atlantic as a western boundary current.

[28] The warmth of Miocene NCW compared to NADW is interesting. It has been previously suggested that saline Tethys outflow increased the salinity of the North Atlantic Ocean and Greenland-Norwegian Seas, permitting the formation of relatively warm NCW [*Schnitker*, 1980]. Alternatively, our results suggest that NCW received its warmth and salinity below the mixed-layer due to a more northeastward orientation of the subtropical gyre and greater mixing by the sub polar gyre. Furthermore, our modeled salinities in the Tethys are not considerably different from other regions at similar latitudes. Thus, our results suggest that NCW may have been warmer and more saline than its modern counterpart without a saline Tethys outflow. Due to the coarse horizontal resolution of the CCSM3 in our study, the Strait of Gibraltar is blocked in the modern bathymetry (Figure 3a). To conserve global salinity, the CCSM3 artificially moves net freshwater fluxes from the Mediterranean Sea to the North Atlantic Ocean at the latitude of the Strait of Gibraltar, over an area of approximately 325,000 km^2. A similar process in the model occurs for all seas isolated from the global ocean. While this is not ideal, it has been shown that, in comparison, explicit parameterization of the Mediterranean overflow has little effect on SSTs (<1.0°C) and the Atlantic meridional overturning circulation [*Wu et al.*, 2007]. Thus comparisons between our Miocene and control cases are not biased by this simplification.

[29] Carbon and oxygen isotope records have been interpreted to indicate the formation of relatively warm saline deep water in the Tethys gateway [*Ramsay et al.*, 1998; *Shevenell and Kennett*, 2004; *Woodruff and Savin*, 1989; *Wright et al.*, 1992]. However, this deep water formation does not occur in our Miocene case. Modeling has demonstrated that substantial low latitude deep water formation is unlikely to have occurred during the Cenozoic, even when considering uncertainties in continental runoff [*Bice and Marotzke*, 2001; *Bice et al.*, 1997]. However, it is necessary to point out that if deep water formation did occur in the Tethys gateway, it may have taken place along shallow margins. The only grid cells in our model with depths less than 100 m lie within the Lago-Mare (Figure 1) and are characterized by low salinities (Figure 3). Thus it would be beneficial to test different river runoff distributions with shallow depth profiles in the Tethys region to see if warm, saline deep water could develop. It is possible that precluding low latitude deep water formation in our simulation has caused convection at other sites (i.e., high latitudes) to compensate.

[30] In addition to warming NCW in our Miocene case, flow from the North Atlantic subtropical gyre enters the Greenland-Norwegian Seas and Arctic basin, mostly between the mixed-layer and 200 m depth (Figure 5d), leading to substantial warming north of 60°N (Figure 11a). The role of the GSR in controlling deep water exchange between the Greenland-Norwegian Seas and global ocean has been the subject of much research and its link to global Neogene climate remains unclear, though is thought to be of secondary importance [*Wright and Miller*, 1996, and references therein]. *Butzin et al.* [2011] show in an ocean model that changes in GSR depth are not required to explain the carbon isotope record in the Atlantic. Consistent with their results, NCW formation does not occur in the Greenland-Norwegian Seas in our Miocene case and thus depth of the GSR would likely not affect overturning circulation. However, the effective removal of the GSR in our bathymetry represents an end-member scenario and, allowing unimpeded exchange between the Greenland-Norwegian Seas and the North Atlantic, has facilitated warming at higher latitudes (Figure 11a). It is likely that with a shallower GSR the flux of subtropical water into the Greenland-Norwegian Seas would be reduced [*Robinson et al.*, 2011]. However, as the poleward flux of subtropical water is larger in the Miocene and occurs at depths less than 1,000 m, we speculate that warmer-than-present sub-surface temperatures would persist in the Greenland-Norwegian Seas if a shallower GSR was prescribed. Furthermore, the lack of deep water formation in the Miocene Greenland-Norwegian Seas limits convective cooling in the region compared to the control case.

[31] The relatively weak NCW formation in the Miocene is attributed in part to fresher surface waters in the North Atlantic, fed by a fresher East Greenland Current (cf. Figures 3 and 9). However, strong cyclonic circulation believed to be necessary for preconditioning the water column at sites of convection [*Marshall and Schott*, 1999] is also limited in the Miocene by a substantially weaker Icelandic low (Figures 6 and 8). Additionally, we associate weakened gyre circulation with greater mixing of warmer subtropical waters below the mixed-layer, reducing the potential density of NCW (not shown). Weakening of the meridional temperature gradient and associated zonal wind stress in the southern hemisphere also reduces global overturning (see below). Thus overturning in the North Atlantic after the middle Miocene would likely have increased with intensification of the subpolar gyre (via growth of the Greenland ice sheet and the associated atmospheric high), southward migration of the eastern flank of the subtropical gyre, cooling and salinization of surface waters and an increase in the meridional temperature gradient.

[32] The root cause of enhanced Weddell Sea bottom water formation cannot be determined without additional sensitivity tests. However, just as convective preconditioning in the North Atlantic is inhibited in the Miocene, conversely, such conditions in the Atlantic sector of the Southern Ocean are enhanced. A significant reduction in sea-ice concentration compared to the present (Figure 4) places the Weddell Sea region under greater influence from surface winds, with the potential to increase cyclonic circulation and surface buoyancy loss, both requirements for deep convection [*Marshall and Schott*, 1999]. An increase in wintertime cyclonic circulation in the Weddell Sea is not simulated in our Miocene case however there is an increase in net outgoing energy of more than 50 W/m^2, suggesting one of the key processes (and feedbacks) to Weddell Sea deep water formation is exposure of the mixed-layer to the atmosphere. It is important to note that in reality modern day deep water forms in the Weddell Sea via downslope convection from the continental shelf and subsequent mixing with the Weddell Sea gyre. Once this water mass mixes with the Weddell Sea gyre it is further cooled via exposure to the atmosphere in the Weddell Sea polynya, and from there undergoes deep convection. The coarse resolution of CCSM3 precludes wintertime cooling along the shelf as well as the Weddell Sea polynya, thus deep water formation due to this process is not represented in our modern simulation (Figure 9a). However, there is no reason to believe that

convection along the continental shelf did not also occur during the Miocene (unless Southern Ocean sea-ice was completely absent) and assuming this was the case the trend in our simulations toward greater deep ocean convection in the Miocene Southern Ocean is robust. In our HiCO2 case, Weddell Sea deep water formation is enhanced as sea-ice concentrations compared to the standard Miocene case are further reduced. This results in greater net outgoing energy (i.e., heat loss) compared to the standard Miocene case over a larger area of the Weddell Sea, and subsequently stronger convection (cf. Figures 9b and 14a).

[33] Peak zonal mean wind stress over the Southern Ocean is approximately 10% weaker in the Miocene (Figure 7) and on average is shifted poleward by approximately 4° compared to the modern. This weakening is a response to reduced transient eddy momentum fluxes (not shown). In contrast, the northern hemisphere midlatitude westerlies increase in the Miocene (Figure 7) due to increased momentum fluxes. Poleward shifts of the surface westerlies have been simulated in both simple and complex aqua-planet models and attributed to, among other changes, increases in global mean temperature [*Lu et al.*, 2010], a result consistent with the poleward shift in both hemispheres seen here. The reduced southern hemisphere westerlies weaken global overturning circulation and most evidently deep water upwelling at the Antarctic divergence (the southern edge of the Deacon cell, Figures 5a and 5b). Ocean model sensitivity tests show that increased Ekman divergence due to strengthening of the southern hemisphere midlatitude westerlies drives stronger global overturning and NADW formation [*Toggweiler and Samuels*, 1995]. Thus, weaker southern hemisphere midlatitude westerlies are a principal cause of the sluggish meridional overturning circulation (Figures 5a and 5b) and NCW formation in our Miocene case (Figure 10).

5.2. Panama Throughflow

[34] *Von der Heydt and Dijkstra* [2006] demonstrate a reversal of Panama throughflow between the Oligocene and Miocene in response to changing widths of the Southern Ocean and Tethys gateways. They conduct Oligocene and Miocene coupled atmosphere–ocean model experiments which include an open and closed Tethys gateway respectively—thus their Miocene geography differs to ours—and show that closure of the Tethys gateway and widening of Southern Ocean gateways changes net volume transport through Panama from westward in the Oligocene (−4.2 Sv) to eastward in the Miocene (16.8 Sv). In contrast, our Miocene case, with the same gateway configuration as their Oligocene simulation, shows a small net eastward transport through the Panama gateway (0.6 Sv; Table 1). Specifically, the upper 100 m experiences westward flow while all other depths experience eastward flow, with the exception of two vertical levels (equal to 1,700 and 2,100 m depth) where net flow is close to zero, but in the westward direction. We note that the gateway in the study of *von der Heydt and Dijkstra* [2006] is open in both the zonal and meridional direction, whereas ours is only open meridionally. Consequently they note eastward throughflow in their simulation is caused by a strengthening and extension of the north equatorial counter current into the Caribbean Sea, which is not possible in our geography. We speculate that this zonal aspect contributed to their significantly larger net volume transports compared to our Miocene and HiCO2 cases. The paleogeography of Central America prior to the closure of the Panama gateway is poorly constrained, however, it is thought that the deep water connection between the Caribbean Sea and the Pacific Ocean during the late early to middle Miocene—which existed at the northwestern edge of the South American plate—had a meridional orientation [*Coates and Obando*, 1996; *Kirby et al.*, 2008]. Shallow water connections likely also existed throughout Central America, though even this is disputed [*Kirby and MacFadden*, 2005]. Thus we believe a meridional orientation of the Panama gateway in global scale simulations is more realistic for the late early to middle Miocene.

5.3. Ocean Heat Transport

[35] Carbon and oxygen isotope interpretations suggest that relatively warm and saline deep water formed in the Tethys gateway and entered the Atlantic basin—analogous to modern Mediterranean outflow—though provided sufficient southward heat transport to inhibit Antarctic ice sheet growth [*Ramsay et al.*, 1998]. Other interpretations suggest Tethys outflow into the Indian Ocean may have also acted as an ocean heat source to Antarctica, subsequently terminating with closure of the eastern portal of the Tethys and concomitant with Miocene cooling [*Ramsay et al.*, 1998; *Woodruff and Savin*, 1989]. Further still, others have suggested that increased ocean heat transport increased high latitude atmospheric moisture, fuelling ice sheet growth in the late Miocene [*Prentice and Matthews*, 1991; *Schnitker*, 1980]. While it has been demonstrated that even extreme changes to ocean heat transport do not proportionately affect continental interior climates [*Huber and Nof*, 2006; *Sloan et al.*, 1995], it should be noted that warm high latitude SSTs need not explain an absence of ice sheets during the Miocene [*Pekar and DeConto*, 2006]. In any case, *Shevenell et al.* [2008] find support for atmospheric moisture feedbacks in a high resolution correlation between middle Miocene ice sheet growth and high Southern Ocean temperatures. The cause of increased ocean heat transport to the high southern latitudes is controversial as numerical models have generally discounted significant low latitude deep water formation during the Cenozoic [*Bice and Marotzke*, 2001; this study]. Our results show that intensification of Weddell Sea bottom water formation is a plausible means for developing warmer-than-present surface air temperatures adjacent to Antarctica. Additionally, the shallower depth of the Kerguelen Plateau in our Miocene bathymetry steers the sub-Antarctic front poleward, (Figure 2). The depth of the Kerguelen Plateau in our Miocene bathymetry is ∼1,000 m, consistent with paleodepth constraints from benthic foraminifera [*Mackensen and Berggren*, 1992]. To our knowledge the effect of Large Igneous Provinces on poleward heat transport has not been examined and should be the focus of future studies. Many studies with idealized bathymetries likely underestimate the impact that these large bathymetric features had in the past when they were younger and shallower. Nevertheless, the majority of net global ocean heat transport increase takes place in the low to middle latitudes (Figure 13) and it is temperatures at sites of deep water formation that predominantly influence benthic proxy data. Thus the persistence of extensive sea-ice in our Miocene simulation ensures

erroneously cool benthic temperatures (Table 2). A further failure of our model is its inability to reproduce warmer-than-present temperatures in the northern Indian Ocean (not shown), inferred from low oxygen isotope ratios [e.g., *Woodruff and Savin*, 1989]. Moreover our results can also not rule out increased sensitivity of the Antarctic ice sheet to changes in orbital forcing, gateway configurations and atmospheric moisture [*Holbourn et al.*, 2005; *Pagani et al.*, 1999; *Shevenell et al.*, 2008].

[36] The high southern hemisphere ocean heat transport in the Miocene compared to the modern is surprising given that the open Drake and Tasman gateways allow for the formation of a strong Antarctic Circumpolar Current (Figures 13 and 6b). *Toggweiler and Bjornsson* [2000] demonstrate in an ocean model that opening of the Drake gateway, even to a moderate depth, causes the onset of strong northern hemisphere overturning. They show that this asymmetry leads to significant high latitude cooling (warming) in the southern (northern) hemisphere. However, their model uses a highly idealized bathymetry composed of a narrow strip of land connecting two polar islands and periodic ocean ridge segments. Our simulations, with more realistic bathymetry and interactive atmospheric coupling, show that northern hemisphere overturning does not dominate ocean heat transport in a realistic Miocene climate model incorporating a deep Drake gateway (Figures 5a and 13). An important oceanographic feature not considered in the experiments of *Toggweiler and Bjornsson* [2000] is the existence of the Panama gateway, which is well known to reduce NADW formation and northern hemisphere surface temperatures [*Butzin et al.*, 2011; *Lunt et al.*, 2008; *Maier-Reimer et al.*, 1990; *von der Heydt and Dijkstra*, 2008]. Therefore the effects of the Drake gateway opening were likely ameliorated by the Panama gateway, which did not close until around the Pliocene [*Molnar*, 2008]. Previous versions of the CCSM used to simulate the climates of the Cretaceous [*Otto-Bliesner et al.*, 2002], Eocene [*Huber et al.*, 2004], Oligocene and early Miocene [*von der Heydt and Dijkstra*, 2006] exhibit similar ocean heat transport anomalies to our study, namely significantly higher southern hemisphere heat transport and lower northern hemisphere heat transport compared to their respective control simulations (each based on modern or pre-industrial boundary conditions). This suggests that the shift to the extant northern hemisphere dominated ocean heat transport was a relatively recent phenomenon and was likely related to closure of the Panama gateway [see also *Butzin et al.*, 2011]. This is consistent with the fact that Northern Hemisphere glaciation occurred much after the middle Miocene when Southern Ocean gateways were unequivocally open.

5.4. Experiment Caveats

[37] The failure of the CCSM3 to reproduce Miocene deep water temperatures is a result of numerous uncertainties in model boundary conditions, proxy records and model physics, and the degree to which each of these contributes to this poor performance deserves discussion. Paleobathymetry is reconstructed by the application of an age-depth relationship to Miocene isochrones overlain with reconstructed large igneous provinces and sediment thicknesses [*Herold et al.*, 2008]. This represents an improvement over classic 'bath tub' style bathymetries [e.g., *Barron and Peterson*, 1991], however, nuances in geology not captured by this method can be important for global climate. Events such as closure of the Tethys gateway are controversial and are thought to be climatically significant [e.g., *Ramsay et al.*, 1998]. As discussed in section 5.1, the depth of the GSR may have had an influential role in the northward flux of water from the subtropics, though likely had little effect on the meridional overturning circulation [*Butzin et al.*, 2011]. The geometry of ocean gateways, which are being reconstructed with increasing accuracy, may also be important to climate, such as the Drake [*Lagabrielle et al.*, 2009; *Sijp and England*, 2004], Panama (discussed in section 5.2) and Indonesian gateways [*Cane and Molnar*, 2001; *Kuhnt et al.*, 2004]. While atmosphere–ocean modeling suggests changes in ocean heat transport have not dominated global temperature changes throughout the Cenozoic [*Huber and Sloan*, 2001; *von der Heydt and Dijkstra*, 2006; this study], regional effects and teleconnections may still have manifested. *Sijp and England* [2004] demonstrate that gradual deepening of the Drake Passage strengthens NADW formation, with an open versus closed configuration cooling South Atlantic SSTs by up to 10°C while warming the North Atlantic by approximately 7°C. *Cane and Molnar* [2001] hypothesize a switch from warm South Pacific Indonesian throughflow to cool North Pacific throughflow with narrowing of the Indonesian gateway, leading to the aridification of Africa. The significance of such geographical changes in the context of Miocene climate can only be properly examined through additional sensitivity experiments. While CO_2 is becoming better constrained [*Beerling and Royer*, 2011], additional radiative forcing may have come from elevated methane concentrations. The lack of a proxy for this greenhouse gas leads to a reliance on chemical modeling, which suggests that methane concentrations were higher than pre-industrial levels during the Miocene [*Beerling et al.*, 2009].

[38] Uncertainty in our model-data analysis stems from the difference in depths between the true paleo ocean floor and modern ocean floor. However, the cold bias shown in Table 2 is consistent with a similar model-data analysis using terrestrial temperature records, which indicates the simulated surface meridional temperature gradient is significantly steeper than suggested by proxy records [*Herold et al.*, 2011]. This result is consistent with previous modeling studies of the Miocene [*Micheels et al.*, 2007; *Steppuhn et al.*, 2007; *Tong et al.*, 2009; *You et al.*, 2009] and other epochs [*Shellito et al.*, 2003; *Sloan and Rea*, 1996].

[39] The prescription of 1950 orbital parameters may also bias interpretations of our results. These values were chosen to be consistent with pre-industrial simulations conducted under the Paleoclimate Modeling Intercomparison Project (http://pmip3.lsce.ipsl.fr/), since our time period of interest is on the order of millions of years long and not dominated by any single orbital configuration. By keeping these parameters at near-modern values we address only the low frequency changes in boundary conditions since the Miocene. However, Earth's current eccentricity is low (i.e., close to a circular orbit) and the northern hemisphere summer solstice is close to aphelion. These two features are not representative of mean orbital conditions. The timing of aphelion in our simulations leads to a considerably weaker northern hemisphere summer insolation compared to most other times in Earths past and thus acts to bias high northern latitudes

toward cooler summer temperatures. A higher eccentricity than prescribed here would amplify this 'cool' northern summer configuration (modulation of precession). Less importantly, a higher eccentricity would increase the mean annual insolation incident on Earth, though this effect is on the order of 0.5 W/m^2 and thus minor. Considering the size of the model-data discrepancies (Table 2) and in the context of other modeling studies of the Miocene [e.g., *Micheels et al.*, 2011; *Steppuhn et al.*, 2007; *Tong et al.*, 2009] and other epochs [e.g., *Huber et al.*, 2003], we do not believe the chosen orbital parameters alter our conclusions.

[40] It is clear that a large deficiency exists in the marriage of climate physics, reconstructed boundary conditions and proxy records at the global scale. While the low resolution CCSM3 is known to have a relatively low CO_2 sensitivity [*Otto-Bliesner et al.*, 2006]—our most ill-constrained boundary condition and one of the most climatically important—we have demonstrated that this is clearly not the sole nor likely the main reason for our simulation's failure to reproduce a warm Miocene ocean. Further, the abundance of proxy data suggesting significant warmth in the Miocene compared to the present (both in the marine and terrestrial realm) makes it highly unlikely that proxy records are providing a misplaced measure of Miocene warmth. Thus, it can be inferred that insufficiencies in the model are the primary cause of discrepancies between our simulations and what is known of Miocene climate. While the low resolution CCSM3 can reproduce modern day climate quite well (compare control case temperature and modern observed temperature columns in Table 2), it seems that its sensitivity to forcing is weak, which is consistent with the emerging view that, in total, general circulation models cannot sufficiently simulate the magnitude of large scale changes to the climate system [e.g., *Valdes*, 2011].

6. Conclusions

[41] We present ocean circulation results from the CCSM3 forced with global Miocene boundary conditions. An additional experiment with a higher CO_2 concentration of 560 ppmv is also examined. Our main findings are summarized below;

1. Our results qualitatively support interpretations of carbon and neodymium isotope records indicating NCW formation in the North Atlantic [*Via and Thomas*, 2006; *Wright et al.*, 1992] as well as a dominant bottom water source in the Southern Ocean [e.g., *Woodruff and Savin*, 1989; *Wright and Miller*, 1993]. However, the strength of NCW in our Miocene case is significantly weaker than inferred by some authors from observations [*Wright et al.*, 1992] and may more closely represent a late Miocene state [*Woodruff and Savin*, 1989]. We find that the primary region of early to middle Miocene bottom water formation is the Weddell Sea. Interestingly, the strength of Weddell Sea bottom water and NCW formation are moderated by CO_2, which suggests that a very weak NCW formation could have existed under significantly higher concentrations than used here. Such a state would be consistent with the hypothesis of negligible NCW formation in the early Miocene [*Woodruff and Savin*, 1989].

2. Global meridional overturning circulation is weaker than present. The main causes of this and the weaker NCW formation are a combination of regional changes in the North Atlantic, primarily weakening of the subpolar gyre, and weaker midlatitude southern hemisphere westerlies. Sensitivity studies are necessary to determine the separate contributions from these. Strong Weddell Sea deep water formation in the Miocene is attributed to reduced sea-ice cover and the subsequent cooling of surface waters.

3. Our simulations fail, spectacularly, to simulate Miocene deep ocean warmth. This suggests significant deficiencies exist in our model boundary conditions, the physics of the CCSM3 and/or the interpretation of proxy records. Together, the insensitivity of the CCSM3 to increased CO_2—our most ill-constrained boundary condition—as well as the diversity of proxy records that indicate Miocene warmth suggest that the major failing lies with the model. The relatively good performance of the model in simulating the present-day ocean may lead to a false sense of confidence in modeling ocean states significantly different to this.

4. NCW is warm and saline compared to modern NADW. This is a result of a northward deflection of North Atlantic subtropical water below the mixed-layer, a weakening of the subpolar gyre and weaker convection, as opposed to warm Tethys outflow [*Schnitker*, 1980].

5. Southern hemisphere ocean heat transport was significantly greater than modern however we find that this was not due to the formation of relatively warm saline deep water in the Tethys [e.g., *Ramsay et al.*, 1998; *Woodruff and Savin*, 1989]. Instead, Weddell Sea bottom water formation, weaker midlatitude westerlies and a shallower Kerguelen Plateau lead to warmer temperatures at high southern latitudes in the Miocene. Our modeled ocean heat transport is qualitatively similar to that simulated by late Cretaceous and early Cenozoic climate models [*Huber and Sloan*, 2001; *Otto-Bliesner et al.*, 2002; *von der Heydt and Dijkstra*, 2006]. This suggests that the shift to the northern hemisphere dominated ocean heat transport of the present occurred after the Miocene climatic optimum and was not a response to opening of the Drake Passage or development of the Antarctic Circumpolar Current.

[42] **Acknowledgments.** This research was undertaken on the NCI National Facility in Canberra, Australia, which is supported by the Australian Commonwealth Government. In addition, parts of this research were funded by NSF grants to M.H., 0450221-EAR and 0902780-ATM. This is PCCRC paper number 1114. We thank J.R. Toggweiler as well as three anonymous reviewers for their help in significantly improving this manuscript. N.H. would like to thank Christine Shields for invaluable technical help and Willem Sijp for helpful discussions.

References

Ali, J. R., and M. Huber (2010), Mammalian biodiversity on Madagascar controlled by ocean currents, *Nature*, *463*(7281), 653–656, doi:10.1038/nature08706.

Backman, J., and K. Moran (2009), Expanding the Cenozoic paleoceanographic record in the Central Arctic Ocean: IODP Expedition 302 Synthesis, *Cent. Eur. J. Geosci.*, *1*(2), 157–175, doi:10.2478/v10085-009-0015-6.

Barron, E. J., and W. H. Peterson (1991), The Cenozoic ocean circulation based on ocean General Circulation Model results, *Palaeogeogr. Palaeoclimatol. Palaeoecol.*, *83*(1–3), 1–28, doi:10.1016/0031-0182(91)90073-Z.

Beerling, D. J., and D. L. Royer (2011), Convergent Cenozoic CO_2 history, *Nat. Geosci.*, *4*(7), 418–420, doi:10.1038/ngeo1186.

Beerling, D., R. A. Berner, F. T. Mackenzie, M. B. Harfoot, and J. A. Pyle (2009), Methane and the CH_4 related greenhouse effect over the past 400 million years, *Am. J. Sci.*, *309*(2), 97–113, doi:10.2475/02.2009.01.

Bice, K. L., and J. Marotzke (2001), Numerical evidence against reversed thermohaline circulation in the warm Paleocene/Eocene ocean, *J. Geophys. Res.*, *106*, 11,529–11,542, doi:10.1029/2000JC000561.

Bice, K. L., E. J. Barron, and W. H. Peterson (1997), Continental runoff and early Cenozoic bottom-water sources, *Geology*, *25*(10), 951–954, doi:10.1130/0091-7613(1997)025<0951:CRAECB>2.3.CO;2.

Bice, K. L., C. R. Scotese, D. Seidov, and E. J. Barron (2000), Quantifying the role of geographic change in Cenozoic ocean heat transport using uncoupled atmosphere and ocean models, *Palaeogeogr. Palaeoclimatol. Palaeoecol.*, *161*(3–4), 295–310, doi:10.1016/S0031-0182(00)00072-9.

Billups, K., and D. P. Schrag (2002), Paleotemperatures and ice volume of the past 27 Myr revisited with paired Mg/Ca and $^{18}O/^{16}O$ measurements on benthic Foraminifera, *Paleoceanography*, *17*(1), 1003, doi:10.1029/2000PA000567.

Bindoff, N. L. et al. (2007), Observations: Oceanic climate change and sea level, in *Climate Change 2007: The Physical Science Basis. Contribution of Working Group I to the Fourth Assessment Report of the Intergovernmental Panel on Climate Change*, edited by S. Solomon et al., pp. 385–432, Cambridge Univ. Press, Cambridge, U. K.

Brady, E. C., R. M. DeConto, and S. L. Thompson (1998), Deep water formation and poleward ocean heat transport in the warm climate extreme of the Cretaceous (80 Ma), *Geophys. Res. Lett.*, *25*(22), 4205–4208, doi:10.1029/1998GL900072.

Butzin, M., G. Lohmann, and T. Bickert (2011), Miocene ocean circulation inferred from marine carbon cycle modeling combined with benthic isotope records, *Paleoceanography*, *26*, PA1203, doi:10.1029/2009PA001901.

Cane, M. A., and P. Molnar (2001), Closing of the Indonesian seaway as a precursor to east African aridification around 3–4 million years ago, *Nature*, *411*(6834), 157–162, doi:10.1038/35075500.

Coates, A. G., and J. A. Obando (1996), The geologic evolution of the Central American Isthmus, in *Evolution of Environments in Tropical America*, edited by J. B. C. Jackson, A. F. Budd, and A. G. Coates, pp. 21–56, Univ. of Chicago Press, Chicago, Ill.

Collins, W. D., et al. (2006), The Community Climate System Model Version 3(CCSM3), *J. Clim.*, *19*(11), 2122–2143, doi:10.1175/JCLI3761.1.

Crowley, T. J., and J. C. Zachos (2000), Comparison of zonal temperature profiles for past warm time periods, in *Warm Climates in Earth History*, edited by B. T. Huber et al., pp. 50–76, Cambridge Univ. Press, Cambridge, U. K., doi:10.1017/CBO9780511564512.004.

Flower, B. P., and J. P. Kennett (1994), The middle Miocene climatic transition: East Antarctic ice sheet development, deep ocean circulation and global carbon cycling, *Palaeogeogr. Palaeoclimatol. Palaeoecol.*, *108*(3–4), 537–555, doi:10.1016/0031-0182(94)90251-8.

Fofonoff, N. P., and R. C. Millard (1983), Algorithms for computation of fundamental properties of seawater, *UNESCO Tech. Pap. Mar. Sci.*, *44*, 53 pp.

Herold, N., M. Seton, R. D. Müller, Y. You, and M. Huber (2008), Middle Miocene tectonic boundary conditions for use in climate models, *Geochem. Geophys. Geosyst.*, *9*, Q10009, doi:10.1029/2008GC002046.

Herold, N., M. Huber, and R. D. Müller (2011), Modeling the Miocene climatic optimum. Part I: Land and atmosphere, *J. Clim.*, *24*, 6353–6372, doi:10.1175/2011JCLI4035.1.

Holbourn, A., W. Kuhnt, M. Schulz, and H. Erlenkeuser (2005), Impacts of orbital forcing and atmospheric carbon dioxide on Miocene ice-sheet expansion, *Nature*, *438*(7067), 483–487, doi:10.1038/nature04123.

Huber, M., and R. Caballero (2011), The early Eocene equable climate problem revisited, *Clim. Past*, *7*(2), 603–633, doi:10.5194/cp-7-603-2011.

Huber, M., and D. Nof (2006), The ocean circulation in the southern hemisphere and its climatic impacts in the Eocene, *Palaeogeogr. Palaeoclimatol. Palaeoecol.*, *231*(1–2), 9–28, doi:10.1016/j.palaeo.2005.07.037.

Huber, M., and L. C. Sloan (2001), Heat transport, deep waters, and thermal gradients: Coupled simulation of an Eocene greenhouse climate, *Geophys. Res. Lett.*, *28*(18), 3481–3484, doi:10.1029/2001GL012943.

Huber, M., L. C. Sloan, and C. Shellito (2003), Early Paleogene oceans and climate: Fully coupled modeling approach using the NCAR CCSM, in *Causes and Consequences of Globally Warm Climates in the Early Paleogene*, edited by S. L. Wing et al., *Spec. Pap. Geol. Soc. Am.*, *369*, 25–47.

Huber, M., H. Brinkhuis, C. E. Stickley, K. Döös, A. Sluijs, J. Warnaar, S. A. Schellenberg, and G. L. Williams (2004), Eocene circulation of the Southern Ocean: Was Antarctica kept warm by subtropical waters?, *Paleoceanography*, *19*, PA4026, doi:10.1029/2004PA001014.

Jakobsson, M., et al. (2007), The early Miocene onset of a ventilated circulation regime in the Arctic Ocean, *Nature*, *447*(7147), 986–990, doi:10.1038/nature05924.

Kiehl, J. T., and C. A. Shields (2005), Climate simulation of the latest Permian: Implications for mass extinction, *Geology*, *33*(9), 757–760, doi:10.1130/G21654.1.

Kirby, M. X., and B. MacFadden (2005), Was southern Central America an archipelago or a peninsula in the middle Miocene? A test using land-mammal body size, *Palaeogeogr. Palaeoclimatol. Palaeoecol.*, *228*(3–4), 193–202, doi:10.1016/j.palaeo.2005.06.002.

Kirby, M. X., D. S. Jones, and B. J. MacFadden (2008), Lower Miocene Stratigraphy along the Panama Canal and Its Bearing on the Central American Peninsula, *PLoS ONE*, *3*(7), e2791, doi:10.1371/journal.pone.0002791.

Klocker, A., M. Prange, and M. Schulz (2005), Testing the influence of the Central American Seaway on orbitally forced Northern Hemisphere glaciation, *Geophys. Res. Lett.*, *32*, L03703, doi:10.1029/2004GL021564.

Knies, J., and C. Gaina (2008), Middle Miocene ice sheet expansion in the Arctic: Views from the Barents Sea, *Geochem. Geophys. Geosyst.*, *9*, Q02015, doi:10.1029/2007GC001824.

Kuhnt, W., A. Holbourn, R. Hall, M. Zuvela, and R. Kaese (2004), Neogene history of the Indonesian throughflow, in *Continent-Ocean Interactions Within East Asian Marginal Seas*, edited by P. D. Clift et al., pp. 299–320, AGU, Washington, D. C., doi:10.1029/149GM16.

Kürschner, W. M., Z. Kvacek, and D. L. Dilcher (2008), The impact of Miocene atmospheric carbon dioxide fluctuations on climate and the evolution of terrestrial ecosystems, *Proc. Natl. Acad. Sci. U. S. A.*, *105*(2), 449–453, doi:10.1073/pnas.0708588105.

Lagabrielle, Y., Y. Goddéris, Y. Donnadieu, J. Malavieille, and M. Suarez (2009), The tectonic history of Drake Passage and its possible impacts on global climate, *Earth Planet. Sci. Lett.*, *279*(3–4), 197–211, doi:10.1016/j.epsl.2008.12.037.

Lear, C. H., H. Elderfield, and P. A. Wilson (2000), Cenozoic deep-sea temperatures and global ice volumes from Mg/Ca in benthic foraminiferal calcite, *Science*, *287*(5451), 269–272, doi:10.1126/science.287.5451.269.

Liu, Z., M. Pagani, D. Zinniker, R. DeConto, M. Huber, H. Brinkhuis, S. R. Shah, R. M. Leckie, and A. Pearson (2009), Global cooling during the Eocene-Oligocene climate transition, *Science*, *323*(5918), 1187–1190, doi:10.1126/science.1166368.

Lu, J., G. Chen, and D. M. W. Frierson (2010), The position of the midlatitude storm track and eddy-driven westerlies in aquaplanet AGCMs, *J. Atmos. Sci.*, *67*(12), 3984–4000, doi:10.1175/2010JAS3477.1.

Lunt, D. J., P. J. Valdes, A. Haywood, and I. C. Rutt (2008), Closure of the Panama Seaway during the Pliocene: Implications for climate and Northern Hemisphere glaciation, *Clim. Dyn.*, *30*(1), 1–18, doi:10.1007/s00382-007-0265-6.

Mackensen, A., and W. A. Berggren (1992), Paleogene benthic foraminifers from the southern Indian Ocean (Kerguelen Plateau): Biostratigraphy and paleoecology, *Proc. Ocean Drill. Program Sci. Results*, *120*, 603–630.

Maier-Reimer, E., U. Mikolajewicz, and T. Crowley (1990), Ocean general circulation model sensitivity experiment with an open Central American isthmus, *Paleoceanography*, *5*(3), 349–366, doi:10.1029/PA005i003p00349.

Marshall, J., and F. Schott (1999), Open-ocean convection: Observations, theory, and models, *Rev. Geophys.*, *37*(1), 1–64, doi:10.1029/98RG02739.

Meehl, G. A., et al. (2007), Global climate projections, in *Climate Change 2007: The Physical Science Basis. Contribution of Working Group I to the Fourth Assessment Report of the Intergovernmental Panel on Climate Change*, edited by S. Solomon et al., pp. 748–845, Cambridge Univ. Press, Cambridge, U. K.

Micheels, A., A. A. Bruch, D. Uhl, T. Utescher, and V. Mosbrugger (2007), A Late Miocene climate model simulation with ECHAM4/ML and its quantitative validation with terrestrial proxy data, *Palaeogeogr. Palaeoclimatol. Palaeoecol.*, *253*(1–2), 251–270, doi:10.1016/j.palaeo.2007.03.042.

Micheels, A., A. A. Bruch, J. Eronen, M. Fortelius, M. Harzhauser, T. Utescher, and V. Mosbrugger (2011), Analysis of heat transport mechanisms from a Late Miocene model experiment with a fully coupled atmosphere–ocean general circulation model, *Palaeogeogr. Palaeoclimatol. Palaeoecol.*, *304*(3–4), 337–350, doi:10.1016/j.palaeo.2010.09.021.

Molnar, P. (2008), Closing of the Central American Seaway and the Ice Age: A critical review, *Paleoceanography*, *23*, PA2201, doi:10.1029/2007PA001574.

Müller, R. D., M. Sdrolias, C. Gaina, and W. R. Roest (2008), Age, spreading rates and spreading asymmetry of the world's ocean crust, *Geochem. Geophys. Geosyst.*, *9*, Q04006, doi:10.1029/2007GC001743.

Najjar, R. G., G. T. Nong, D. Seidov, and W. H. Peterson (2002), Modeling geographic impacts on early Eocene ocean temperature, *Geophys. Res. Lett.*, *29*(15), 1750, doi:10.1029/2001GL014438.

Nisancioglu, K. H., M. E. Raymo, and P. H. Stone (2003), Reorganization of Miocene deep water circulation in response to the shoaling of the Central American Seaway, *Paleoceanography*, *18*(1), 1006, doi:10.1029/2002PA000767.

Nong, G. T., R. G. Najjar, D. Seidov, and W. H. Peterson (2000), Simulation of ocean temperature change due to the opening of Drake Passage, *Geophys. Res. Lett.*, *27*(17), 2689–2692, doi:10.1029/1999GL011072.

Oleinik, A., L. Marincovich, K. B. Barinov, and P. K. Swart (2008), Magnitude of middle Miocene warming in North Pacific high latitudes: Stable isotope evidence from Kaneharaia (Bivalvia, Dosiniinae), *Bull. Geol. Surv. Jpn.*, *59*(7–8), 339–353.

Otto-Bliesner, B. L., E. C. Brady, and C. Shields (2002), Late Cretaceous ocean: Coupled simulations with the National Center for Atmospheric Research Climate System Model, *J. Geophys. Res.*, *107*(D2), 4019, doi:10.1029/2001JD000821.

Otto-Bliesner, B. L., R. Tomas, E. C. Brady, C. Ammann, Z. Kothavala, and G. Clauzet (2006), Climate sensitivity of moderate- and low-resolution versions of CCSM3 to preindustrial forcings, *J. Clim.*, *19*(11), 2567–2583, doi:10.1175/JCLI3754.1.

Pagani, M., M. A. Arthur, and K. H. Freeman (1999), Miocene evolution of atmospheric carbon dioxide, *Paleoceanography*, *14*(3), 273–292, doi:10.1029/1999PA900006.

Pekar, S. F., and R. M. DeConto (2006), High-resolution ice-volume estimates for the early Miocene: Evidence for a dynamic ice sheet in Antarctica, *Palaeogeogr. Palaeoclimatol. Palaeoecol.*, *231*(1–2), 101–109, doi:10.1016/j.palaeo.2005.07.027.

Poore, H. R., R. Samworth, N. J. White, S. M. Jones, and I. N. McCave (2006), Neogene overflow of Northern Component Water at the Greenland-Scotland Ridge, *Geochem. Geophys. Geosyst.*, *7*, Q06010, doi:10.1029/2005GC001085.

Prentice, M. L., and R. K. Matthews (1991), Tertiary ice sheet dynamics: The snow gun hypothesis, *J. Geophys. Res.*, *96*(B4), 6811–6827, doi:10.1029/90JB01614.

Ramsay, A. T. S., C. W. Smart, and J. C. Zachos (1998), A model of early to middle Miocene deep ocean circulation for the Atlantic and Indian oceans, in *Geological Evolution of Ocean Basins: Results From the Ocean Drilling Program*, edited by M. B. Hart, *Geol. Soc. Spec. Publ.*, *131*, 55–70, doi:10.1144/GSL.SP.1998.131.01.04.

Robinson, M. M., P. J. Valdes, A. M. Haywood, H. J. Dowsett, D. J. Hill, and S. M. Jones (2011), Bathymetric controls on Pliocene North Atlantic and Arctic sea surface temperature and deepwater production, *Palaeogeogr. Palaeoclimatol. Palaeoecol.*, *309*(1–2), 92–97, doi:10.1016/j.palaeo.2011.01.004.

Sangiorgi, F., H.-J. Brumsack, D. A. Willard, S. Schouten, C. E. Stickley, M. O'Regan, G.-J. Reichart, J. S. Sinninghe Damsté, and H. Brinkhuis (2008), A 26 million year gap in the central Arctic record at the greenhouse-icehouse transition: Looking for clues, *Paleoceanography*, *23*, PA1S04, doi:10.1029/2007PA001477.

Savin, S. M., R. G. Douglas, and F. G. Stehli (1975), Tertiary marine paleotemperatures, *Geol. Soc. Am. Bull.*, *86*, 1499–1510, doi:10.1130/0016-7606(1975)86<1499:TMP>2.0.CO;2.

Schnitker, D. (1980), North Atlantic oceanography as possible cause of Antarctic glaciation and eutrophication, *Nature*, *284*(5757), 615–616, doi:10.1038/284615a0.

Shackleton, N. J., and J. P. Kennett (1975), Paleotemperature history of the Cenozoic and the initiation of Antarctic glaciation; oxygen and carbon isotope analyses in DSDP sites 277, 279, and 281, *Initial Rep. Deep Sea Drill. Proj.*, *29*, 743–755.

Shellito, C. J., L. C. Sloan, and M. Huber (2003), Climate model sensitivity to atmospheric CO_2 levels in the Early Middle Paleogene, *Palaeogeogr. Palaeoclimatol. Palaeoecol.*, *193*(1), 113–123, doi:10.1016/S0031-0182(02)00718-6.

Shellito, C. J., J.-F. Lamarque, and L. C. Sloan (2009), Early Eocene Arctic climate sensitivity to pCO_2 and basin geography, *Geophys. Res. Lett.*, *36*, L09707, doi:10.1029/2009GL037248.

Shevenell, A., and J. Kennett (2004), Paleoceanographic change during the Middle Miocene climate revolution: An Antarctic stable isotope perspective, in *The Cenozoic Southern Ocean: Tectonics, Sedimentation, and Climate Change Between Australia and Antarctica*, *Geophys. Monogr. Ser.*, vol. 151, edited by N. F. Exon, J. P. Kennett, and M. J. Malone, pp. 235–251, AGU, Washington, D. C., doi:10.1029/151GM14.

Shevenell, A. E., J. P. Kennett, and D. W. Lea (2008), Middle Miocene ice sheet dynamics, deep-sea temperatures, and carbon cycling: A Southern Ocean perspective, *Geochem. Geophys. Geosyst.*, *9*, Q02006, doi:10.1029/2007GC001736.

Sijp, W. P., and M. H. England (2004), Effect of the Drake Passage throughflow on global climate, *J. Phys. Oceanogr.*, *34*(5), 1254–1266, doi:10.1175/1520-0485(2004)034<1254:EOTDPT>2.0.CO;2.

Sijp, W. P., M. H. England, and J. R. Toggweiler (2009), Effect of Ocean gateway changes under greenhouse warmth, *J. Clim.*, *22*(24), 6639–6652, doi:10.1175/2009JCLI3003.1.

Sloan, L. C., and D. K. Rea (1996), Atmospheric carbon dioxide and early Eocene climate: A general circulation modeling sensitivity study, *Palaeogeogr. Palaeoclimatol. Palaeoecol.*, *119*(3–4), 275–292, doi:10.1016/0031-0182(95)00012-7.

Sloan, L. C., J. C. G. Walker, and T. C. Moore Jr. (1995), Possible role of oceanic heat transport in early Eocene climate, *Paleoceanography*, *10*(2), 347–356, doi:10.1029/94PA02928.

Stein, C. A., and S. Stein (1992), A model for the global variation in oceanic depth and heat flow with lithospheric age, *Nature*, *359*(6391), 123–129, doi:10.1038/359123a0.

Steppuhn, A., A. Micheels, A. Bruch, D. Uhl, T. Utescher, and V. Mosbrugger (2007), The sensitivity of ECHAM4/ML to a double CO_2 scenario for the Late Miocene and the comparison to terrestrial proxy data, *Global Planet. Change*, *57*(3–4), 189–212, doi:10.1016/j.gloplacha.2006.09.003.

St. John, K. (2008), Cenozoic ice-rafting history of the central Arctic Ocean: Terrigenous sands on the Lomonosov Ridge, *Paleoceanography*, *23*, PA1S05, doi:10.1029/2007PA001483.

Toggweiler, J. R., and H. Bjornsson (2000), Drake Passage and palaeoclimate, *J. Quaternary Sci.*, *15*(4), 319–328, doi:10.1002/1099-1417(200005)15:4<319::AID-JQS545>3.0.CO;2-C.

Toggweiler, J. R., and B. Samuels (1995), Effect of Drake Passage on the global thermohaline circulation, *Deep Sea Res., Part I*, *42*(4), 477–500, doi:10.1016/0967-0637(95)00012-U.

Tong, J. A., Y. You, R. D. Müller, and M. Seton (2009), Climate model sensitivity to atmospheric CO_2 concentrations for the middle Miocene, *Global Planet. Change*, *67*(3–4), 129–140, doi:10.1016/j.gloplacha.2009.02.001.

Valdes, P. (2011), Built for stability, *Nat. Geosci.*, *4*(7), 414–416, doi:10.1038/ngeo1200.

Via, R. K., and D. J. Thomas (2006), Evolution of Atlantic thermohaline circulation: Early Oligocene onset of deep-water production in the North Atlantic, *Geology*, *34*(6), 441–444, doi:10.1130/G22545.1.

von der Heydt, A., and H. A. Dijkstra (2006), Effect of ocean gateways on the global ocean circulation in the late Oligocene and early Miocene, *Paleoceanography*, *21*, PA1011, doi:10.1029/2005PA001149.

von der Heydt, A., and H. A. Dijkstra (2008), The effect of gateways on ocean circulation patterns in the Cenozoic, *Global Planet. Change*, *62*(1–2), 132–146, doi:10.1016/j.gloplacha.2007.11.006.

Warny, S., R. A. Askin, M. J. Hannah, B. A. R. Mohr, J. I. Raine, D. M. Harwood, F. Florindo, and SMS Science Team (2009), Palynomorphs from a sediment core reveal a sudden remarkably warm Antarctica during the middle Miocene, *Geology*, *37*(10), 955–958, doi:10.1130/G30139A.1.

Wolfe, J. A. (1985), Distribution of major vegetational types during the Tertiary, in *The Carbon Cycle and Atmospheric CO_2: Natural Variations Archean to Present*, *Geophys. Monogr. Ser*, vol. 32, edited by E. T. Sundquist and W. S. Broecker, pp. 357–375, AGU, Washington, D. C., doi:10.1029/GM032p0357

Woodruff, F., and S. M. Savin (1989), Miocene deepwater oceanography, *Paleoceanography*, *4*(1), 87–140, doi:10.1029/PA004i001p00087.

Wright, J. D., and K. G. Miller (1993), Southern Ocean influences on late Eocene to Miocene deepwater circulation, *Antarct. Res. Ser.*, *60*, 1–25, doi:10.1029/AR060p0001.

Wright, J. D., and K. G. Miller (1996), Control of North Atlantic Deep Water circulation by the Greenland-Scotland Ridge, *Paleoceanography*, *11*(2), 157–170, doi:10.1029/95PA03696.

Wright, J. D., K. G. Miller, and R. G. Fairbanks (1992), Early and middle Miocene stable isotopes; implications for deepwater circulation and climate, *Paleoceanography*, *7*(3), 357–389, doi:10.1029/92PA00760.

Wu, W., G. Danabasoglu, and W. G. Large (2007), On the effects of parameterized Mediterranean overflow on North Atlantic ocean circulation and climate, *Ocean Modell.*, *19*(1–2), 31–52, doi:10.1016/j.ocemod.2007.06.003.

Yeager, S. G., C. A. Shields, W. G. Large, and J. J. Hack (2006), The low-resolution CCSM3, *J. Clim.*, *19*(11), 2545–2566, doi:10.1175/JCLI3744.1.

You, Y., M. Huber, R. D. Müller, C. J. Poulsen, and J. Ribbe (2009), Simulation of the Middle Miocene Climate Optimum, *Geophys. Res. Lett.*, *36*, L04702, doi:10.1029/2008GL036571.

Zachos, J. C., G. R. Dickens, and R. E. Zeebe (2008), An early Cenozoic perspective on greenhouse warming and carbon-cycle dynamics, *Nature*, *451*(7176), 279–283, doi:10.1038/nature06588.

N. Herold, R. D. Müller, and M. Seton, EarthByte Group, School of Geosciences, University of Sydney, Sydney, NSW 2006, Australia. (nher5224@uni.sydney.edu.au)

M. Huber, Earth and Atmospheric Sciences, Purdue University, 1397 Civil Engineering Bldg., West Lafayette, IN 47906, USA.